AD A062 021 MASSACHUSETTS INST OF TECH CAMBRIDGE DEPT OF ELECTRI--ETC F/G 17/2
AN INVESTIGATION OF ATMOSPHERIC OPTICALLY SCATTERED NON-LINE-OF--ETC(U)
OCT 78 W S ROSS DAAG29-77-C-0048
UNCLASSIFIED ARO-15365.1-A-EL NL

1 OF 1
AD A062 021

END
DATE FILMED
3 -- 79
DDC

Unclassified

SECURITY CLASSIFICATION OF THIS PAGE (When Data Entered)

REPORT DOCUMENTATION PAGE

READ INSTRUCTIONS BEFORE COMPLETING FORM

1. REPORT NUMBER: 15365.1-A-EL (18) ARO	2. GOVT ACCESSION NO.
3. RECIPIENT'S CATALOG NUMBER: (9)	
4. TITLE (and Subtitle): An Investigation of Atmospheric Optically Scattered Non-Line-of-Sight Communication Links.	5. TYPE OF REPORT & PERIOD COVERED: Final Report. 26 Sep 77 - 26 Sep 78,
6. PERFORMING ORG. REPORT NUMBER	
7. AUTHOR(s): Warren S. Ross (10)	8. CONTRACT OR GRANT NUMBER(s): (15) DAAG29-77-C-0048
9. PERFORMING ORGANIZATION NAME AND ADDRESS: Massachusetts Institute of Technology, Cambridge, Massachusetts 02139	10. PROGRAM ELEMENT, PROJECT, TASK AREA & WORK UNIT NUMBERS: (12) 58p.
11. CONTROLLING OFFICE NAME AND ADDRESS: U. S. Army Research Office, P. O. Box 12211, Research Triangle Park, NC 27709 (11)	12. REPORT DATE: October 1978
	13. NUMBER OF PAGES: 54
14. MONITORING AGENCY NAME & ADDRESS (if different from Controlling Office)	15. SECURITY CLASS. (of this report): Unclassified
	15a. DECLASSIFICATION/DOWNGRADING SCHEDULE

LEVEL II

16. DISTRIBUTION STATEMENT (of this Report)

Approved for public release; distribution unlimited.

DDC RECEIVED DEC 11 1978 F

17. DISTRIBUTION STATEMENT (of the abstract entered in Block 20, if different from Report)

18. SUPPLEMENTARY NOTES

The view, opinions, and/or findings contained in this report are those of the author(s) and should not be construed as an official Department of the Army position, policy, or decision, unless so designated by other documentation.

19. KEY WORDS (Continue on reverse side if necessary and identify by block number)

Optical Communications
Cambridge Experiment
Lubec Experiment
Communication Links
Optical Communication System Design
Communications Systems
Atmosphere

20. ABSTRACT (Continue on reverse side if necessary and identify by block number)

This report contains the results of a study of short-haul non-line-of-sight optical communication. The experimental facilities are discussed and include source description, receiver description, post-detection processing, and ozone measurements. Cambridge and Lubec experiments were performed. The experimental results include measurement of weather conditions, angular spreading, and non-line-of-sight data. Future research is also discussed.

DD FORM 1 JAN 73 1473 EDITION OF 1 NOV 65 IS OBSOLETE

Unclassified 220 015

FINAL REPORT

(SIXTY COPIES REQUIRED)

1. ARO PROPOSAL NUMBER: _____

2. PERIOD COVERED BY REPORT: September 26, 1977 - September 26, 1978

3. TITLE OF PROPOSAL: An Investigation of Atmospheric Optically Scattered Non-Line-of-Sight Communication Links

4. CONTRACT OR GRANT NUMBER: Contract DAAG29-77-C-0048

5. NAME OF INSTITUTION: Massachusetts Institute of Technology

6. AUTHOR(S) OF REPORT: Warren S. Ross

7. LIST OF MANUSCRIPTS SUBMITTED OR PUBLISHED UNDER ARO SPONSORSHIP DURING THIS PERIOD, INCLUDING JOURNAL REFERENCES:

   None

8. SCIENTIFIC PERSONNEL SUPPORTED BY THIS PROJECT AND DEGREES AWARDED DURING THIS REPORTING PERIOD:

   Scientific Personnel

   R. S. Kennedy, Professor

   J. J. Shapiro, Associate Professor

   H. P. Jensen, Research Associate

   W. Ross, Research Assistant

Dr Robert S. Kennedy
Massachusetts Institute of Technology
Department of Electrical Engineering
and Computer Science
Cambridge Ma 02139

AN INVESTIGATION OF ATMOSPHERIC OPTICALLY SCATTERED NON-LINE-OF-SIGHT COMMUNICATION LINKS

U.S. Army Research Office

Contract DAAG29-77-C-0048

FINAL REPORT

covering the period

September 26, 1977 - September 26, 1978

Submitted by: Warren S. Ross

Principal Investigator: Robert S. Kennedy

September 26, 1978

Massachusetts Institute of Technology

Research Laboratory of Electronics

Cambridge Massachusetts 02139

TABLE OF CONTENTS

LIST OF FIGURES

ACKNOWLEDGEMENTS

List of Personnel

Faculty: Robert S. Kennedy

Students: Warren S. Ross
Louis A. Nagode
Mahmoud Tebyani

We also wish to acknowledge the support of those who helped us in our experimental field trip to Lubec, Maine, particularly Ernest Brierly and the Urquhart family.

1.0 Introduction

Short-haul non-line-of sight optical communication is the subject of the investigation discussed in this report. The long range goal of the investigation is to provide the foundation for the design of an alternative (optical) communication system for short-range non-line-of-sight communication in cities and built-up areas. [1-4].

A requirement of optical communication system design and analysis is knowledge of the statistical properties of the received field. These properties are determined by the propagation characteristics of the atmosphere as well as by the specific communication link geometry and the transmitted optical field. Absorption and scattering by atmospheric constituents (molecular and aerosol) corrupt the transmitted optical field. The relation between the quantity (and distribution) of these atmospheric constituents and the statistics of the received field is very complicated, particularly in low-visibility weather condition (haze, rain, fog, snow, etc.) where multiple-scattering predominates.

It is known that in multiple-scattering conditions the received field envelope is a zero-mean complex Gaussian random process [5], so that the field statistics are entirely characterized by the space-time correlation function. However, this correlation function is itself impossible to determine in general.

Fortunately, the entire function is not needed for communication system design. Experience with other types of scatter channels shows that for these purposes, knowledge of a few statistical parameters of the received field will be adequate. [1,5]. These parameters are:

1) total average received energy per unit transmitted energy
2) average multipath time spread
3) average angular spectrum width
4) average Doppler spread

Even with this level of simplification, it is a major task to specify the channel parameters for all situations of interest. Theoretically, a complete description of channel propagation is given by the linear transport equation [6,7]. In the minor scattering (single-scattering) and severe scattering (diffusion) extremes, it is straightforward to solve this equation [8,9]. Also, for media in which very sharp forward scattering predominates, other approaches have produced analytical descriptions [10,11]. However, except for these extreme cases, no general solutions currently exist.

It is clear that some knowledge of the channel behavior must be known before theoretical solutions are possible. This fact has motivated us to experimentally determine the channel parameters, in the hope of obtaining enough knowledge about them to make simplifications to the transport equation. Already we have had some success with this approach. Recent experiments at visible and infrared wavelengths demonstrate that the angular spectrum is very narrow over large ranges of optical thickness. This narrowness has been exploited to solve the transport equation and obtain explicit expressions for the channel parameters of interest [12].

Despite these advances, there is no guarantee that the angular spectrum behavior at visible and infrared wavelengths carries over into other wavelength regions. The wavelength region considered for the work reported here is the middle ultraviolet (2000Å-3000Å). The advantages of this region for the application of interest are: invisibility (tactical security), absence of solar background, and availability of good detectors. Hence we have initiated an experimental program to study the angular spectrum in the middle uv, as well as to measure the other channel parameters of interest.

We shall report here on our experimental studies of the middle uv angular spectrum and our experiments with non-line-of-sight propagation in a city environment.

2.0 Experimental

This chapter describes our experimental program to measure the parameters which characterize the low visibility atmospheric channel. Line-of-sight experiments were conducted at two locations:

1) Cambridge, Massachusetts, using our experimental laboratory on the roof of MIT's Earth and Planetary Sciences Building (Green Building);

2) Lubec, Maine, during a field trip which we made from July 24 through August 11.

In addition to these line-of-sight experiments, measurements were made in Cambridge with obstructions in the path. The sections below describe in more detail our experimental facilities and the experiments performed.

2.1 Experimental Facilities

2.1.1 Source Description

All of our measurements to date have been made with a mercury vapor germicidal lamp. This source emits a nominal 1.4 watts of power at 2537Å. The lamp is a 9" long cylindrical bulb which is mounted on an aluminum backing plate to distribute the lamp power over a 2π steradian solid angle (See Fig. 2-1).

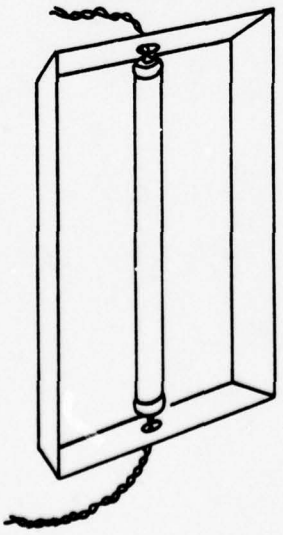

Fig. 2-1: UV Lamp and Reflector

The lamp is normally current modulated using 60 hz line current and a suitable ballast arrangement. However, A.C. power was not available for the source during some of the experiments in Lubec, Maine. Thus it was necessary to operate the lamp using D.C. power with a commercially available D.C.-A.C. inverter (See Fig. 2-2). The photo-control switch shown in Fig. 2-2 was used to save battery power during daylight when experiments were not performed.

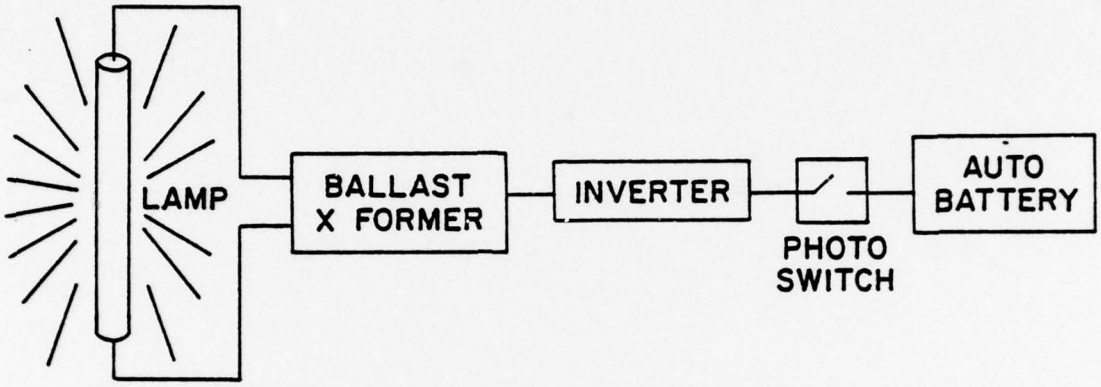

Fig. 2-2: D.C. Operation of Mercury Vapor Lamp

In addition to the mercury vapor lamp, the quadrupled Nd:YAG laser will soon be available as a second source. The laser will emit a 12 nanosecond pulse of 2650Å light with pulse energy of 1-3 millijoule. The beam divergence will be 10 m rad and the pulse rate will be 20 pps. This source will make it possible to measure multipath time spread of the channel, as well as providing increased dynamic range for energy and angular spectrum measurements.

2.1.2 Receiver Description

Three receivers were used for the experiments. Two of them - a variable narrow field-of-view (NFOV) receiver and a fixed wide field-of-view (WFOV) receiver - were built at MIT. The third is a variable WFOV receiver which was borrowed from Honeywell Electro-Optics Division in Lexington, Mass. The specifications for the three receivers are shown in Table 2-1. The mechanical structure of the three receivers is shown in Fig. 2-3.

TABLE 2-1 Receiver Specifications

	Optics	PMT Characteristics
Variable NFOV Receiver	Reflecting telescope: - mirror reflectivity ≈ 90% - focal length = 46" Aperture: 4 1/4" diam. FOV: Variable from < 1 to 20 mr by change of pinhole at focal plane Filter: Dielectric, 7% transmission at 2537 Å	Bialkali cathode QE = 22% at 2537 Å Gain = 2.5×10^7 @ 1400 MHV
Fixed WFOV Receiver	Aperture: 4 1/2" diam. FOV: Controlled by length of pipe on front of PMT, Set at ≈ 17° (FAFOV) Filter: $NiSO_4$ + Cation X solution: 10% transmission at 2537 Å.	RbTe Cathode QE = 8.6 % at 2537 Å Gain = 2.6×10^7 @ 2000 PHV
Variable WFOV Receiver (Honeywell)	Aperture: 1" diam. FOV: Controlled by pipe size on front of PMT: either 22° or 84° (FAFOV) Filter: Solid $NiSO_4$ + Cation X: 2.3% at 2537 Å, completely solar blind.	CsTe Cathode Q.E. = 6.4% at 2537 Å

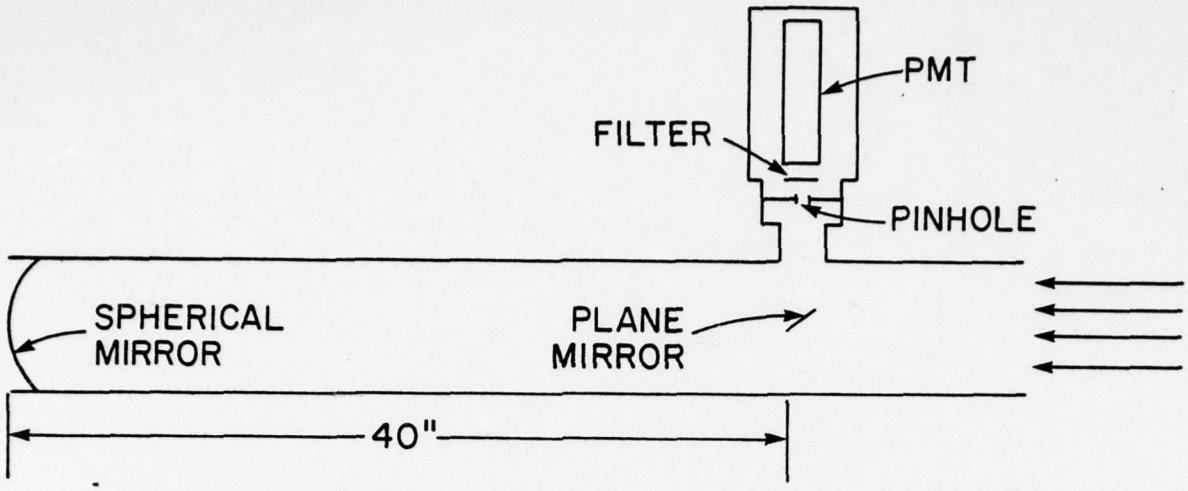

Fig. 2-3a: Variable NFOV Receiver

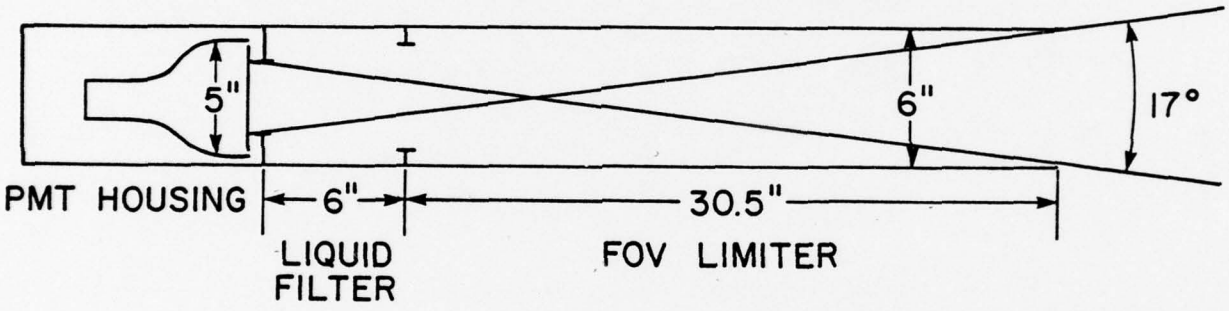

Fig. 2-3b: Fixed WFOV Receiver

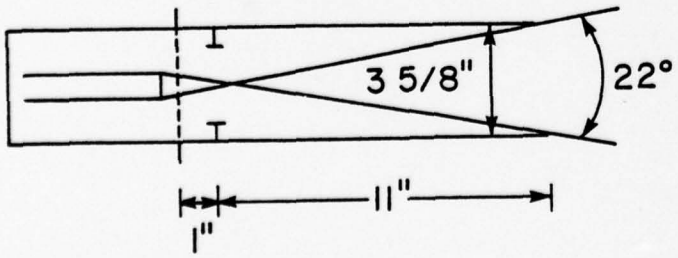

Fig. 2-3c: Honeywell Receiver (Small FOV)

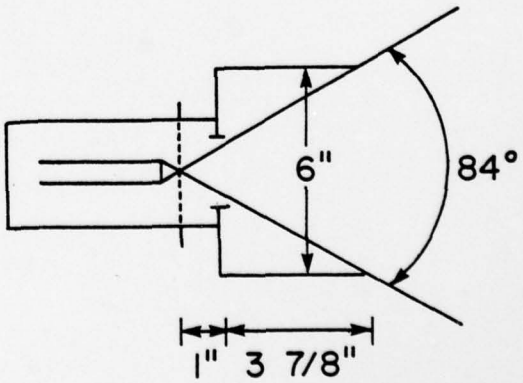

Fig. 2-3d: Honeywell Receiver (Large FOV)

The Honeywell receiver differs from the other two in that a high voltage converter and a pulse amplifier/discriminator are built right into the PMT housing. Thus this receiver can operate off of a 28 volt battery. When combined with a battery operated counter, the Honeywell system is completely portable.

2.1.3 Post-Detection Processing

The output of all three receivers is processed by photon counting. As stated above, the Honeywell receiver has a built-in pulse amplifier/discriminator. The discriminator output is fed to a Fluke Model 1900A multi-counter, provided by Honeywell, which can operate from 60 hz A.C. or batteries. The two other receivers share the same photon counting circuitry. The Laser Sciences Model PC 610 photon counter was used for some of the experiments in Cambridge, but it was damaged prior to the Lubec field excursion. During the Lubec experiments we used the Princeton Applied Research Model 1121 Amplifier/Discriminator combined with the Model 1109 Counter. The output of the counter was recorded either manually or on a strip-chart, depending on the experiment.

2.1.4 Ozone Measurements

We are currently renting the Mast Development Company Model 724-5 Ozone Meter, in order to make in situ measurements of atmospheric ozone concentration. For long term measurement, the ozone concentration is recorded on a strip-chart. Otherwise, the meter reading is simply recorded manually at the time of the experiment.

2.2 Experiments Performed

As stated above, line-of-sight measurements were made in both Cambridge, Mass., and Lubec, Maine. However, because of the significant differences in terrain, pathlength and weather encountered, the Cambridge and Lubec experiments are best described separately.

2.2.1 Cambridge Experiments

The line-of-sight Cambridge experiments were conducted over a one mile path between our laboratory on the roof of the Green Building at MIT and a four story apartment building at 209 Hamilton Street, Cambridge. The source was mounted on the roof

of 209 Hamilton Street and the receivers were located at the Green Building (See Fig. 2-4).

From Fig. 2-4, it is clear that the terrain between source and receivers is a city environment with no body of water along the path (although the source is within a half mile of the Charles River). The structures along the path are mainly 2-4 story buildings. The significance of these facts is in their influence upon four factors which affect our measurements:

1) Background light level - Because of numerous streetlamps and other sources of light within the city, the WFOV system is plagued by considerable background noise, even at night;

2) Ozone sources - Industrial sources contribute to the ozone level as well as natural generation;

3) Prevailing Weather - Fog over the city of Cambridge is very rare. There is a heavy haze that develops over the area during summer days, but it generally dissipates at night;

4) Boundary conditions - Because of buildings and other structures within the city, the ground is not a smooth plane but consists of jagged, irregular boundaries.

The three basic kinds of line-of-sight data obtained were:

1) Receiver elevation scan with 1.35 mr FOV;

2) Signal vs. FOV using 1.35, 2.7, 4.1 and 16.3 mr FOV in the NFOV receiver;

3) NFOV (1.35 mr) signal vs. WFOV (17^{o}) signal.

In addition to the line-of-sight measurements, non-line-of-sight measurements were made using Honeywell's portable sensor. With

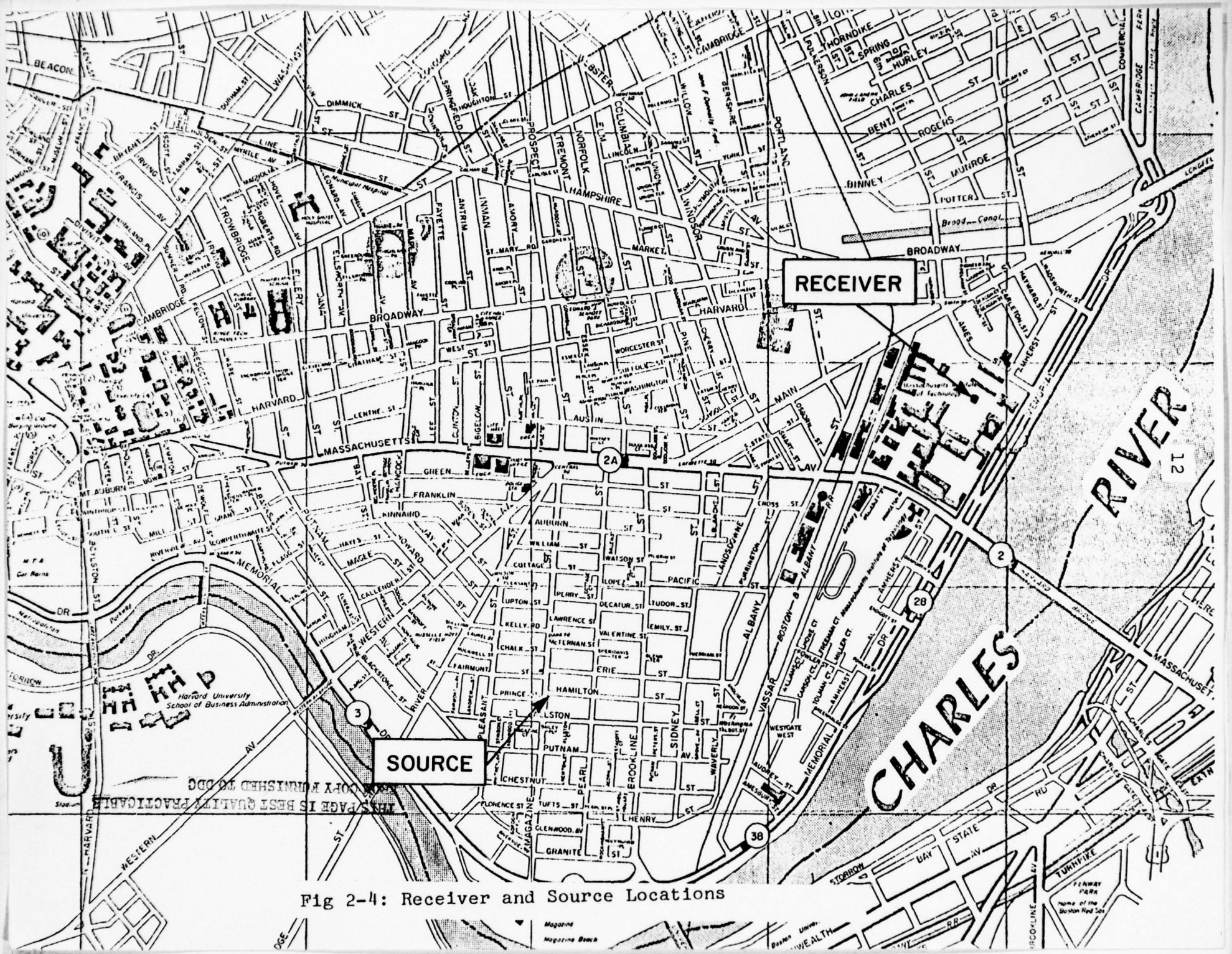

Fig 2-4: Receiver and Source Locations

the source mounted atop 209 Hamilton Street (pointing at the Green Building as usual), measurements were made from various points on the ground. The line of sight to the source was obstructed by buildings and trees during these experiments. The purpose was to get a qualitative idea of the detectability of uv light in a typical city environment. These excursions were made on two occasions, once at night and once during the day. In both cases, the weather was clear.

The amount of line-of-sight data obtained in Cambridge is small, primarily due to the scarcity of very low visibility weather conditions (Visibility ≈ 1 mile or less). Since we did not yet have a highly collimated uv source, it was not possible to take advantage of hazy weather by increasing the length of the path: the $1/r^2$ losses from the semi-isotopic source and the ozone losses would be prohibitive. It was this situation which motivated us to look for an experimental environment in which fog was a more frequent occurence, an environment which we found in Lubec, Maine.

2.2.2 Lubec Experiments

The Lubec, Maine, experiments were conducted during a three week period from July 24 through August 11. The site for the experiments was a small bay called Bailey's Mistake. Fig. 2-5 shows the location of Lubec and a blow-up of the Bailey's Mistake inlet. The receivers were located at point A in Fig. 2-5b. The initial source location was point B in the Figure, approximately a 1 mile pathlength. However, because at that distance we did not have enough dynamic range to measure any signals in the heaviest fog, we moved the source closer (to point C). This final source location is an island approximately 1000 feet from the receivers' location. About two-thirds of that distance is over water.

The terrain on the Bailey's Mistake link is markedly different than that in Cambridge. With reference to the four factors discussed above:

1) Background light level - There were only two streetlamps on Bailey's Mistake and

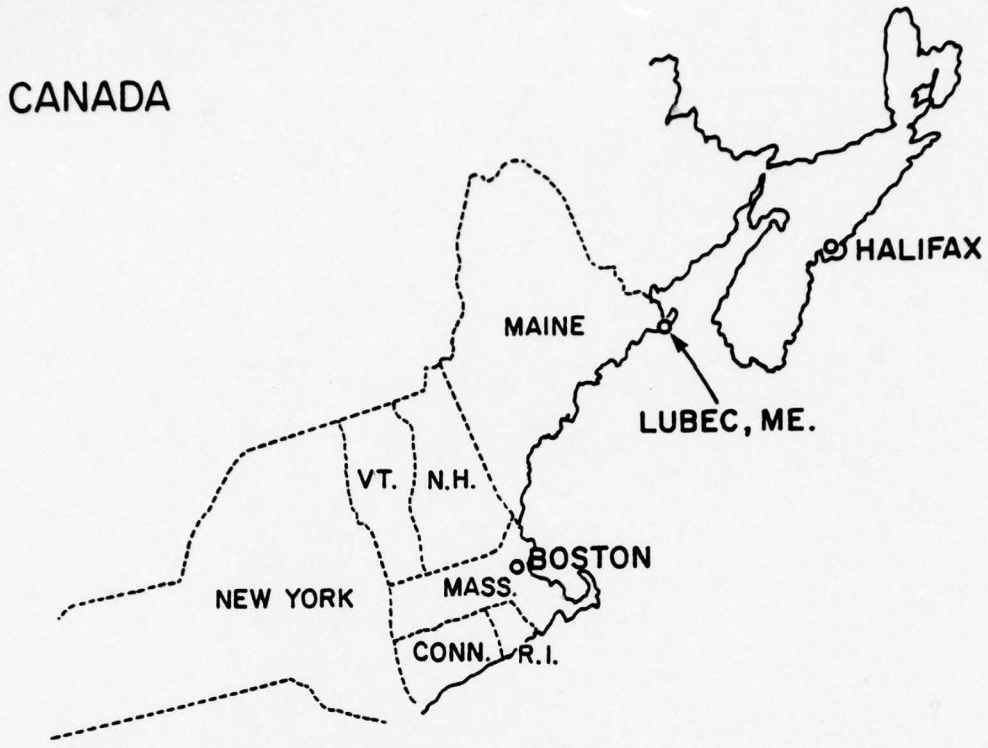

Fig. 2-5a: Location of Lubec, Maine

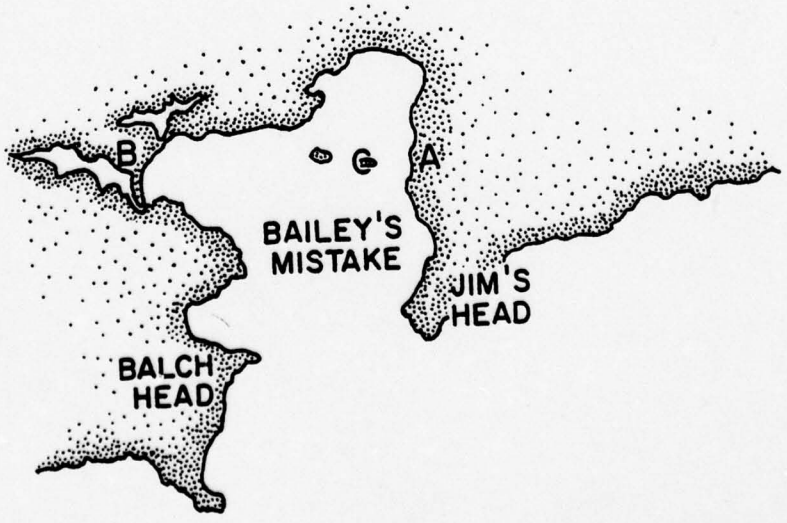

Fig. 2-5b Bailey's Mistake Inlet

both were outside the FOV of the NFOV receiver and the 17° FOV receiver. Hence at night there was no background noise to contend with.

2) Ozone sources - There is negligible industrial contribution to the ozone level. After dark, the ozone concentration was quite low and very steady. (This can also be attributed partly to the high relative humidity in fog.)

3) Prevailing Weather - The relative humidity was often very high and Bailey's Mistake had heavy fog for 8 out of the 19 days spent there. This was true even when there was not a great deal of fog further inland.

4) Boundary conditions - Both source and receivers were within 50 feet of sea level with no buildings or other structures along the path. Hence, the ground and the water's surface can be considered a smooth (perhaps partially reflecting) plane.

The line-of-sight measurements performed at Bailey's Mistake were:

1) Azimuth and elevation angular scans with the NFOV receiver for various fields of view ranging from 1.35 mr to 16.3 mr.

2) Received signal vs. FOV with

   a) NFOV receiver using fields of view ranging from 1.35 mr to 16.3 mr.

   b) Honeywell's receiver - using fields of view ranging from 8.3° to 22°. The fields of view below 22°

were obtained by placing cardboard field stops at different diameters at the front end of the 11" FOV limiting tube (See Fig. 2-6). The 84° FOV was obtained using the configuration in Fig. 2-3d.

3) NFOV signal vs. WFOV signal with both the Honeywell receiver and the 17° FOV receiver alternating as the WFOV system.

4) Crude azimuth scans using the Honeywell receiver with a 180° FAFOV.

5) Signal level vs. FOV using the Honeywell sensor looking off axis (vertical) while changing between three fields of view: 22°, 84° and 180°.

No non line-of-sight measurements were made at Bailey's Mistake.

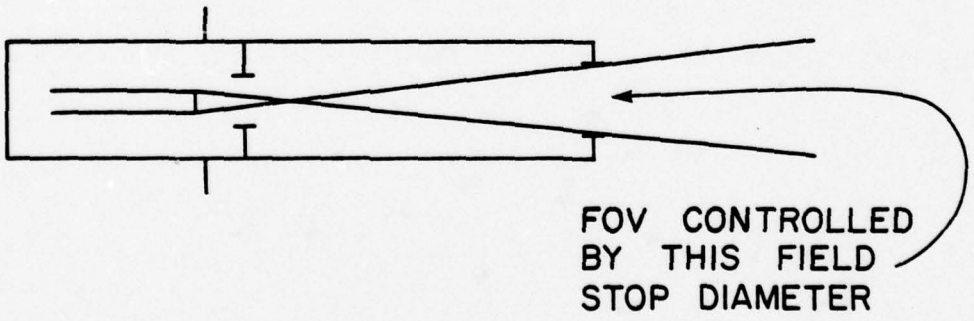

Fig. 2-6: Honeywell Receiver used for FOV Measurements

3.0 Discussion of Experimental Results

The major findings of our experimental program to date will be presented in this chapter, with particular emphasis on the angular spectrum data. The discussion will be a summary, with references made to selected experimental records in Appendix A where appropriate. As a prelude to a discussion of the data, Section 3.1 will consider how the data is to be related to the weather conditions at the time of measurement.

3.1 Measurement of Weather Conditions

Ideally, the atmospheric conditions could be obtained by simple measurements of a few observable parameters. For optical experiments in the visible portion of the spectrum, it is common to assume negligible atmospheric absorption and to characterize the atmospheric conditions by the visibility range. In this region of the spectrum, there is a simple relationship between visible range and extinction [13].

In the middle ultraviolet, however, no such simple relationship exists. Ozone absorption is significant at these wavelengths, so that clear weather extinction could change dramatically depending on the ozone concentration. Furthermore, there is no reason to believe that the scattering coefficient has the same relationship to visibility as it does in the visible. In fact, some experimental evidence indicates that the relationship is not the same [14]. Hence, before visibility information can be of any quantitative value in determining ultraviolet extinction, the exact relationship needs to be determined.

For almost all of our measurements, the atmospheric conditions were characterized by:

1) a general verbal discription (e.g. "haze", "fog", "clear"):

2) an ozone concentration measurement;

3) an extinction measurement.

In some of the experiments in Cambridge, visibility range data was also obtained, for the purpose of determining its relationship to extinction. However, this data was obtained from Logan

Airport and proved to be unreliable: Logan is 3 1/2 miles from our path, and visibility was often noticeably less in the direction of the airport than on our path.

For the experiments in Lubec, during which fog was the prevailing weather condition, the extinction measurement alone was sufficient. The ozone concentration was low enough in fog (and the path was short enough) to make ozone absorption negligible. For this reason, most of the discussion below will be in terms of extinction, or more specifically in terms of the optical thickness.

When angular scans were made with the 1.35 mr FOV, extinction was measured directly by comparing the signal level received on axis with the signal level received on axis in clear weather. When angular scans were made with larger fields of view, there was not sufficient time to change pinholes to make a 1.35 mr extinction measurement directly. In these cases, prediction of the optical thickness was made using a formula derived empirically from the signal vs. FOV data. This formula relates the on-axis signal in a 1.35 mr FOV to that in any other FOV between 1.35 mr and 16.3 mr.

3.2 Angular Spreading

Negligible angular spreading was observed in the experiments in Cambridge, due to the aforementioned lack of foggy weather conditions. The worst weather condition for which we have data in Cambridge was a light fog on May 15, 1978 (Optical thickness about 3.) Figures A-1 and A-2 compare a clear weather elevation scan with the light fog scan. These scans were made with a 1.35 mr FOV. Although there is a slight angular broadening in light fog, it is not more than 1-2 mr at the 1/100th power point.

This conclusion about neglibible angular broadening is supported by signal vs. FOV measurements with the NFOV system. For all measurements made in Cambridge, the power collected with the 1.35 mr FOV was essentially the same as that collected with 2.7 and 4.1 mr. An increase of about 10% in collected power was observed from the 4 mr FOV to 16.3 mr FOV. A typical signal vs. FOV record is shown in Fig. A-3.

There was significantly more angular spreading observed in the heavy fog data obtained in the Lubec experiments. For these

experiments the optical thickness ranged between 5 and 11.

A typical elevation scan with a 1.35 mr FOV is shown in Fig. A-4. Note that several measurements were made on-axis and that the data points are numbered and lettered. These labels indicate the time sequence of the measurement. This time sequencing is valuable in drawing conclusions about the nature of the scan with highly variable unscattered component. (This will be discussed further below).

From a study of the available data, the following are the significant features of the angular spectrum in fog:

1) There is a measureable on-axis signal peak for optical thicknesses below 9. (See Figs A-5 through A-7);

2) This on-axis peak disappears for optical thicknesses greater than about 10, and a uniform angular spectrum results. (See Figs A-6, A-7, A-8).[Note that here time sequencing is very important. For example, in Fig. A-8, it is significant that the on-axis measurement corresponding to the data numbered (12)-(18) is point (15) rather than, say, point (20).

3) For optical thicknesses between 5 and 7, the angular spectrum magnitude is down by a factor of 10 between $\pm$ 5 and $\pm$ 10 mr. (See Figs A-4, A-9, A-11, A-12, A-15). For larger optical thickness, there is a tendency for the spectrum to broaden, until it flattens out as described above (See Figs A-4, A-10);

4) The angular spectrum outside $\pm$ 10 mr is relatively insensitive to changes in the on-axis signal level. It is relatively uniform, with a gradual drop-off. (See Figs A-5, A-13, A-14). The slope of this drop-off is

dependent on optical thickness and becomes slower as optical thickness increases (compare Figs A-13 and A-15).

5) The relatively uniform portion of the angular spectrum extends over a considerable range, at least as far out as 25°. After 5°, this portion of the angular spectrum slopes off at a rate of about 3 dB for each 5° - 10° in angle. At 25 degrees the angular spectrum is down from the peak by 20-30 dB. (See Figs A-13, A-14.)

With these properties as a guide, Fig. 3-1 shows representative angular spectra for three regimes of optical thickness:

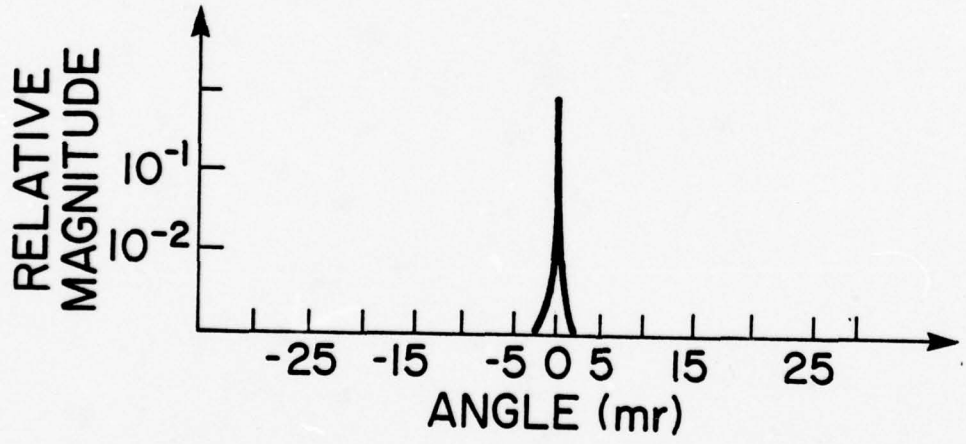

Fig. 3-1a: Angular Spectrum for $\tau < 2$

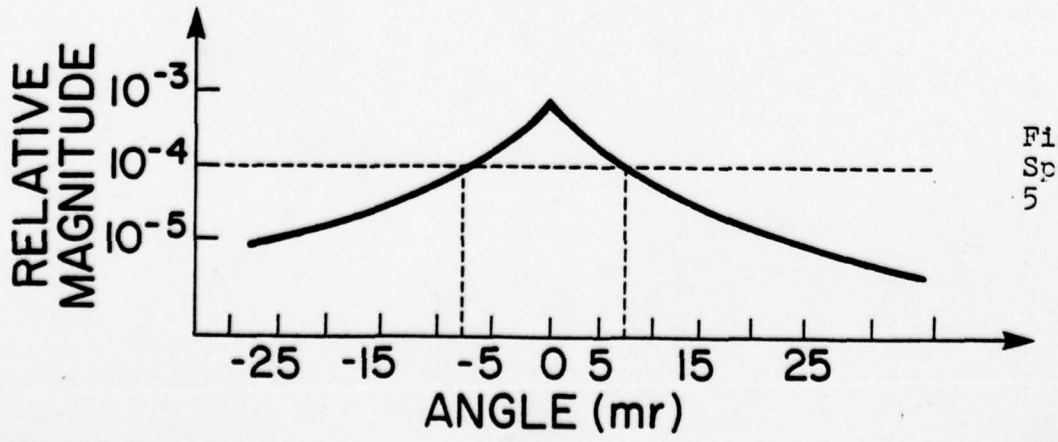

Fig. 3-1b : Angular Spectrum for $5 < \tau < 9$

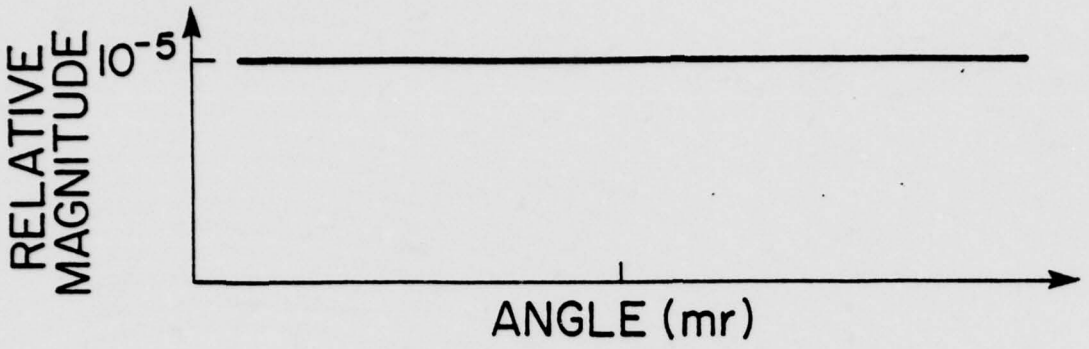

Fig. 3-1c: Angular Spectrum for $\tau > 10$

The signal vs. FOV data obtained in fog is consistent with the above conclusions. Figs A-16 and A-17 are typical experimental records. Note that for optical thicknesses less than 9, there is definitely signal energy outside a few milliradians, but that there is significantly less than would be predicted with a uniform angular spectrum. This comparison is shown graphically in Fig. 3-2, in which the signal vs. FOV data is normalized to the 1.35 mr FOV signal level.

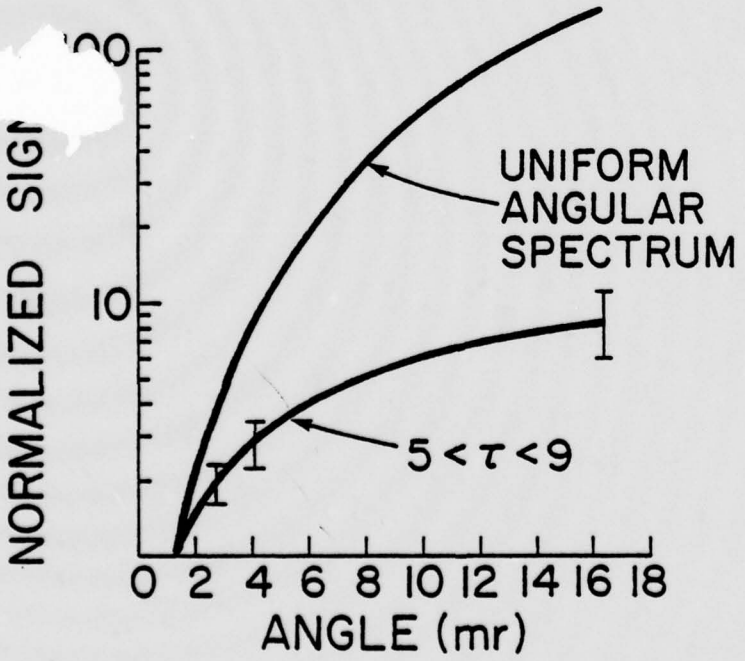

Fig. 3-2: Comparison of Signal vs. FOV Data with Uniform Angular Spectrum Prediction

Unfortunately, no reliable signal vs. FOV data was obtained for optical thicknesses greater than 9. Thus, we could not see if the signal vs. FOV data for an optical thickness of 10 would indeed have fallen along the upper curve in Fig. 3-2 as predicted. However, the lower curve in Fig. 3-2 does shift upward with increasing optical thickness, indicating that an increasing amount of the received energy is being converted from the unscattered to the uniformly scattered component of the angular spectrum.

Despite the qualitative conclusions that have been discussed in this Section, there are still a number of unanswered questions about the behavior of the angular spectrum. First of all, no data has been obtained for optical thicknesses between 3 and 5. The data we have is either for relatively clear weather or for foggy weather. Thus we have no idea about the transition from the impulsive angular spectrum in Fig. 3-1a to the broadened one in Fig 3-1b. Secondly, very little angular scan data and no signal vs. FOV data was obtained for optical thicknesses equal to or longer than 10. This would be helpful as a confirmation of our conclusions above about the onset of a uniform spectrum. Finally, more data needs to be obtained in the range of optical thicknesses between 8 and 10, in order to give us a better idea of the transition from the non-uniform angular spectrum to a uniform one. As stated above, there is some indication in the signal vs. FOV data that this transition is a smooth one in which more and more signal energy is converted from unscattered to uniformly scattered as the optical thickness increases. This conclusion needs to be confirmed. It is our intention to resolve these remaining issues within the coming year, so that our characterization of the angular spectrum will be complete.

We conclude this Section with a discussion of the NFOV (1.35 mr) vs. WFOV (17^{o} or 22^{o}) measurements. The purpose of these measurements was to give a direct comparison of a large collecting angle receiver under identical weather conditions. We would expect to see the WFOV receiver perform increasingly better than a NFOV receiver as the visibility is lowered, as a result of the WFOV receiver's ability to detect a larger proportion of the scattered incident power.

The NFOV vs. WFOV data obtained at Lubec is shown in Figs A-18, A-19, A-20. Except for the 1 mile path data shown in Fig. A-18, the data obtained is only over a small range of possible signal levels. It is still possible, however, to draw a number of conclusions form the data. Most important is that the change in WFOV signal is much smaller than a given change in the NFOV signal. The NFOV signal changes by a factor of 60-90 for a factor of 10 change in the 17° FOV receiver and by a factor of 450 for a factor of 10 change in the 22° FOV receiver.

The relationship is almost linear on log-log coordinates over a wide range of the data obtained. The data in Fig. A-19 indicates that there will be a steepening of the curve as the optical thickness gets smaller, since a straight line plotted through the data at large optical thickness falls below the clear weather data point. There is no evidence of this in Figs A-18 and A-20, however, so this is a question that must still be resolved.

Finally, note that none of the data shown in Figs A-18 through A-20 is consistent with a uniform angular spectrum. For example, the 17° FOV system has a FOV 210 times as large as the NFOV receiver, so that a uniform angular spectrum would give a factor of 44,000 increase in signal in the larger FOV. Yet in Fig A-19 the largest increase (occuring for NFOV signal ≈ 200 c/s, corresponding to $\tau \approx 10$) is only a factor of 65. (Note that this ratio is obtained by first correcting for the factor of 2.7 difference in the clear weather WFOV vs. NFOV measurements).

This is in contradiction to the statement above that for optical thickness around 10, the angular spectrum is uniform. But note that the data on which that conclusion is based (Fig. A-8) only covers a narrow range of angle ($\pm$ 12 mr). It is quite possible that the angular spectrum is uniform for a while, then slopes off enough, so that the increase in received signal is not nearly in proportion to the increase in FOV.

3.3 Non-Line-of-Sight Data

Non-line-of-signt experiments were conducted in Cambridge on two occasions, using Honeywell's portable sensor system. The purpose of these measurements was to determine the amount of signal

that could be received in a typical city environment. With the source mounted on the roof of 209 Hamilton Street, measurements of signal level were made at various points in the city within a mile of the source. The sensor FAFOV was 84°.

Fig. 3-3 is a map of Cambridge with the various measurement locations indicated. Table 3-1 is a comparison of the data obtained on the two occasions. The numbers in parentheses are the distances, in feet, from the source to the measurement point. For comparison purposes, two types of measurement are shown: The "at source" measurement was made with the detector pointed on what would have been a direct line-of-sight if no buildings had obstructed the path. The "straight up" measurement was made with the detector looking straight up at the sky.

On both occasions, an attempt was made to stay at least 20 feet from any building blocking the line-of-sight. At closer distances than this, very little signal could be measured. As expected, this close to a building the "straight up" signal was much larger than the "at source" signal, due to energy being received from the scattering volume above the building. The data obtained on the two dates agree within a factor of 2-3, and constitute a good baseline for comparison with foggy weather measurements when we can make them. From the clear weather data, it is obvious that there is detectable non-line-of-sight signal in clear weather. More importantly there is generally no more than a factor of 5-10 decrease in the "straight up" signal as compared with the "at source" signal. This means that even in clear weather, a wide FOV receiver on the ground in a city environment sees a roughly uniform distribution of signal with angle, and hence pointing is not a severe problem. We expect this uniformity to be even more pronounced in lower visibility conditions

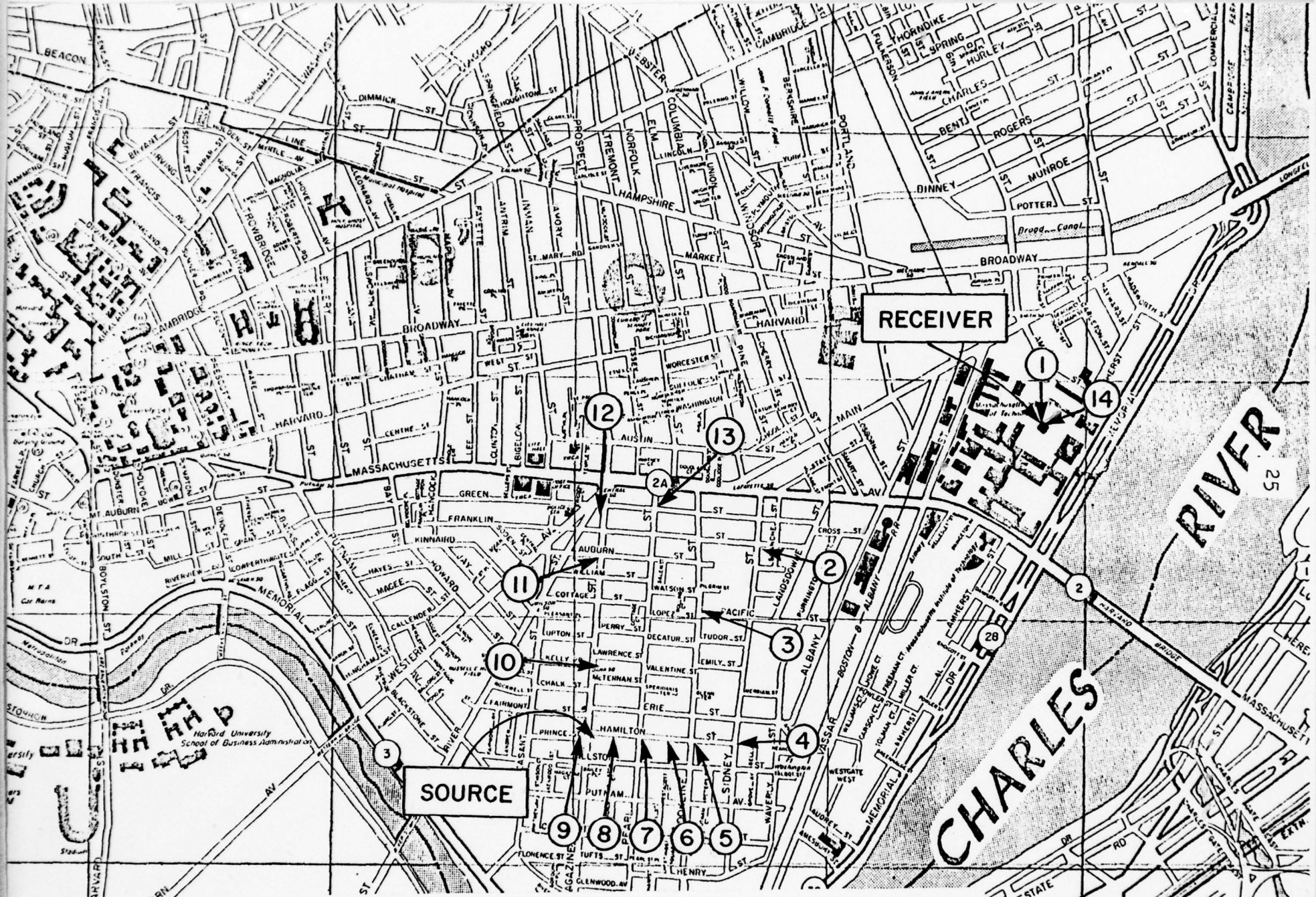

Fig. 3-3: Non-line-of-sight Measurement Locations

TABLE 3-1

Comparison of Non-Line-of-Sight Data

	Location (Dist. in feet)	Detector to Source		Straight Up	
		Feb 20 (counts/sec)	May 4 (counts/sec)	Feb 20 (counts/sec)	May 4 (counts/sec)
1.	Green Bldg (5280) (line-of-sight)	2.2	1-1.1 K	-	30-40
2.	Franklin & Sidney (2400)	1.6 K	1.1 K	500	300
3.	Sidney & Pacific (2400)	2.8-3 K	3700	440	800
4.	Sidney & Hamilton (1300)	5.4 K	3.3 K	1.0-1.2 K	1.2-1.3 K
5.	Brookline & Hamilton (850)	3.2-3.4 K	4.6-4.7 K	800-1 K	2.6 K
6.	Hamilton, betw Pearl & Brookline (575)	8 K	13-14 K	-	4.2 K
7.	Hamilton & Pearl (300)	15 K	26 K	4 K	9 K
8.	190 Hamilton ST (125)	18 K	33 K	6 K	16 K
9.	Magazine & Hamilton (behind source 25-50 ft)	20 K	16 K	-	700

Table 3-1 (cont'd)

Comparison of Non-line-of-Sight Data

	Location (Dist. in feet)	Detector to Source		Straight Up	
		Feb 20 (counts/sec)	May 4 (counts/sec)	Feb 20 (counts/sec)	May 4 (counts/sec)
10.	Magazine & Lawrence (650)	16 K	5.8-6.3 K	2 K	1.6 K
11.	Magazine & Auburn (1650)	20 K	550-600	-	450-500
12.	Magazine & Green (2100)	1.6 K	900-1100	-	250-300
13.	Mass Ave & Pearl (2400)	320	750-800	160	175-200
14.	Green Bldg Roof line-of-sight (5250)	800-1 K	2.5 K	50	

4.0 Future Directions

This chapter will discuss the goals of our research for the upcoming year, including experiments we plan to make, modifications to existing equipment and theoretical work.

4.1 Experiments

Foremost among our experimental goals for the upcoming year will be a continuation of the current experiments to answer the remaining questions about the angular spectrum behavior. Because of the success of the Lubec field trip and the infrequent occurence of heavy fog in the Cambridge area, we plan to make another field trip to a foggy location for the bulk of these experiments. We have not decided whether to return to the Maine coast. The choice will depend on the availability and suitability of experimental sites that are closer to Boston.

In addition to angular spectrum measurements, the quadrupled Nd:YAG laser will be used to make multipath measurements. Initially, the experiments will be made over a short path (1 mile). If there is neglibible time spreading over this pathlength, the path will be extended so that scattering from haze becomes significant. Because of the high collimation of the YAG laser, the pathlength can be increased without suffering prohibitive $1/r^2$ losses.

It will still be desirable to get multipath data in heavy fog. Because the Nd:YAG laser cannot be moved for a field experiment, a field trip necessitates finding a portable narrow pulse source. A possible candidate is a Hg-Xe arc lamp, which has pulsewidths around 1 μsec. Although this is much wider than the 12 n sec Nd:YAG pulse, the multipath spread we expect to see in heavy fog (at least in the diffusion regime) is on the order of 100 μ sec. Hence the 1 μsec pulsewidth should be sufficient.

The third major type of experiment planned for the coming year is a comparison of uv and He Ne laser extinction for the purpose of relating uv extinction to visible range. This experiment will be performed at both 2537Å and 2650Å. The He Ne laser transmitter is already built, having been used for previous experiments. The receiver for both uv and He Ne signal will be the current NFOV

system, modified to make it easy to select He Ne or uv wavelength bands.

Besides line-of-sight experiments, two types of non-line-of-sight experiments will be conducted: one will be a continuation of the signal level measurements in the city of Cambridge. These measurements will be made in low visibility conditions, and comparisons made with the clear weather data. The second type of non-line-of-sight experiment will involve simplified boundary conditions, such as a single large building between source and receiver. This will be for the purpose of comparing with Monte Carlo simulations we plan to make (See Section 4.3 below).

4.2 Modifications to Existing Equipment

Two major modifications to the receivers are planned for the upcoming year. The first is a conversion of both the NFOV receiver and the 17° FOV receiver to completely solar blind systems. As mentioned in Section 3.2.1, the WFOV system has high background noise even at night. Although the NFOV system currently has tolerable background levels at night, it is severely background limited in the daytime. The necessity to operate the systems at night not only cuts the possible data collection time in half, but it also encounters problems with availability of personnel and access to experimental facilities. With solar blind systems, we would still collect data at night, but the ability to experiment in the daytime would be of significant value.

The NFOV receiver would be converted using a solid $NiSO_4$/Cation X filter borrowed from Honeywell. This filter has 1% transmission at 2537Å. and can be mounted on our existing NFOV telescope with some mechanical modifications. Conversion of the WFOV receiver will require purchase of a specially made 5-6" diameter solid filter.

The second major modification planned is an automation of the FOV change on the NFOV receiver. At present, the FOV is changed manually by changing the pinhole at the focal plane of the telescope. This is a time-consuming process, and on a number of occasions we have had to throw out signal vs. FOV data because the weather had changed substantially while a pinhole was being changed. The modification planned is the replacement of the pinhole with an electric iris diaphragm. In addition to allowing a quick manual change of the FOV, an

electric iris will permit unattended signal vs. FOV data collection.

4.3 Theoretical

The theoretical work planned for the next year falls into categories: development and refinement of a propagation theory, and Monte Carlo simulation.

The angular spectrum data we obtain will be used to confirm and refine the tentative description of the angular spectrum given in Chapter 3. In conjunction with the signal vs. FOV data, this data will help us develop a complete understanding of the process by which the impulsive clear weather angular spectrum transforms into a uniform angular spectrum. The multipath data will give us additional confirmation of the angular spectrum description as well as providing the basis for a description of time spreading. Both diffusion regime and single-scatter calculations will be performed to facilitate our understanding. The single-scatter calculations may be especially valuable in explaining the reasonably narrow angular spectrum spike ($\pm$ 10 mr) which was observed in heavy fog.

The Monte Carlo computations will supplement the single-scatter and diffusion calcuations. If we find that the angular spectrum measured in fog cannot adequately be explained as predominantly due to single-scatter, then Monte Carlo simulation will provide a tool to explore this regime. The simulations will be used both to confirm the data and to give us information about areas where data is unavailable.

In addition to line-of-sight Monte Carlo computations, simulation will be used to explore non-line-of-sight propagation. The purpose here will be to make quantitative conclusions about uv propagation in the presence of obstacles and irregular boundaries such as buildings. Rather than try to include all of the complexities of a typical city environment, however, the simulation will be tailored to a very simple geometry, such as a source and receiver on either side of a single building. This geometry should provide enough information to make some conclusions about propagation in more complicated environments.

Even with this severe simplification in boundary conditions, a considerable amount of development work needs to be performed on the

existing Monte Carlo program. In its current form, it is designed to handle propagation through an infinite parallel-plane slab, with no provisions for any boundary conditions. Some of this development has already begun and will continue in the next few months.

References

1. R. S. Kennedy, "Communication through Optical Scattering Channels: An Introduction", Proc. IEEE, vol 58, No. 10, pp 1651-1665, October 1970.

2. R. M. Lerner and A. E. Holland, "The Optical Scatter Channel", Proc. IEEE, Vol. 58, No. 10, pp 1547-1563, October 1970.

3. E. A. Bucher and R. M. Lerner, "Experiments on Light Pulse Communication and Propagation through Atmospheric Clouds", Applied Optics, Vol. 12, No. 10, pp 2404-2414, October, 1973.

4. E. S. Fishburne, M. E. Neer, and G. Sandri, "Voice Communication via Scattered Ultraviolet Radiation", A.R.A.P. Report No. 274, Vol. 1, U.S. Army Electronics Command, Fort Monmount, New Jersey, February, 1976

5. R. S. Kennedy, Fading Dispersive Communication Channels, New York, Wiley, 1969.

6. K. M. Case and P. F. Zweifel, Linear Transport Theory, Addison Wesley Publishing Co., Reading, Massachusets, 1967.

7. R. W. Preisendorfer, Radiative Transfer on Discrete Spaces, Pergamon Press, New York, 1965.

8. D. M. Reilly, "Atmospheric Optical Communications in the Middle Ultraviolet", M.S. Thesis, Department of Electrical Engineering and Computer Science, MIT, May 1976.

9. R. W. Preisendorfer, Hydrologic Optics, Vol III, U.S. Department of Commerce, National Oceanic and Atmospheric Administration, PB-259-795, 1976, pp 175-183.

10. H. M. Heggestad, "Optical Communication through Multiple Scattering Media", Technical Report No. 474, Research Laboratory of Electronics, MIT, Nov. 22, 1968.

11. D. Arnush, "Underwater Light Beam Propagation in the Small-Angle-Scattering Approximation", Journal of the Optical Society of America, Vol. 62, September 1972, pp 1109-1111.

12. R. S. Kennedy and J. H. Shapiro, "Multipath Dispersion in Low Visibility Optical Communication Channels", Final Report, Contract No. F19628-76-C-0054, Rome Air Development Center, Hanscom Air Force Base, Bedford, Massachusetts, January 1977.

13. RCA Electro-Optics Handbook, Technical Series EOH-11, 1974, Chapter 7.

14. J. M. Schlupf, et al, "Seasonal Variations of Single-Scattering Phase Functions in the Ultraviolet, A.R.A.P. Report, July 1978.

APPENDIX:

Selected
Experimental
Records

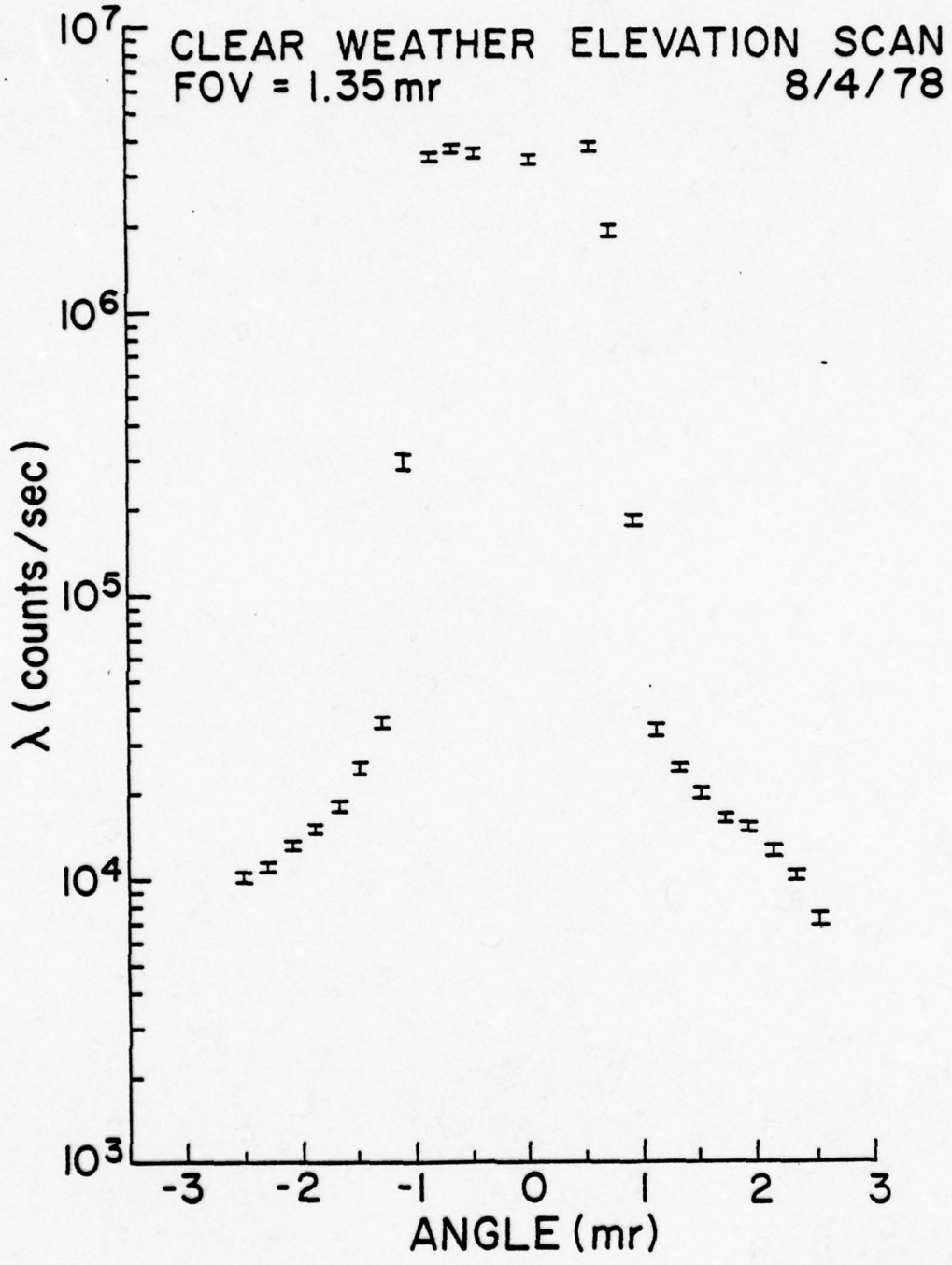
CLEAR WEATHER ELEVATION SCAN
FOV = 1.35 mr
8/4/78
λ (counts/sec)
10^7
10^6
10^5
10^4
10^3
-3
-2
-1
0
1
2
3
ANGLE (mr)

Fig. A-1

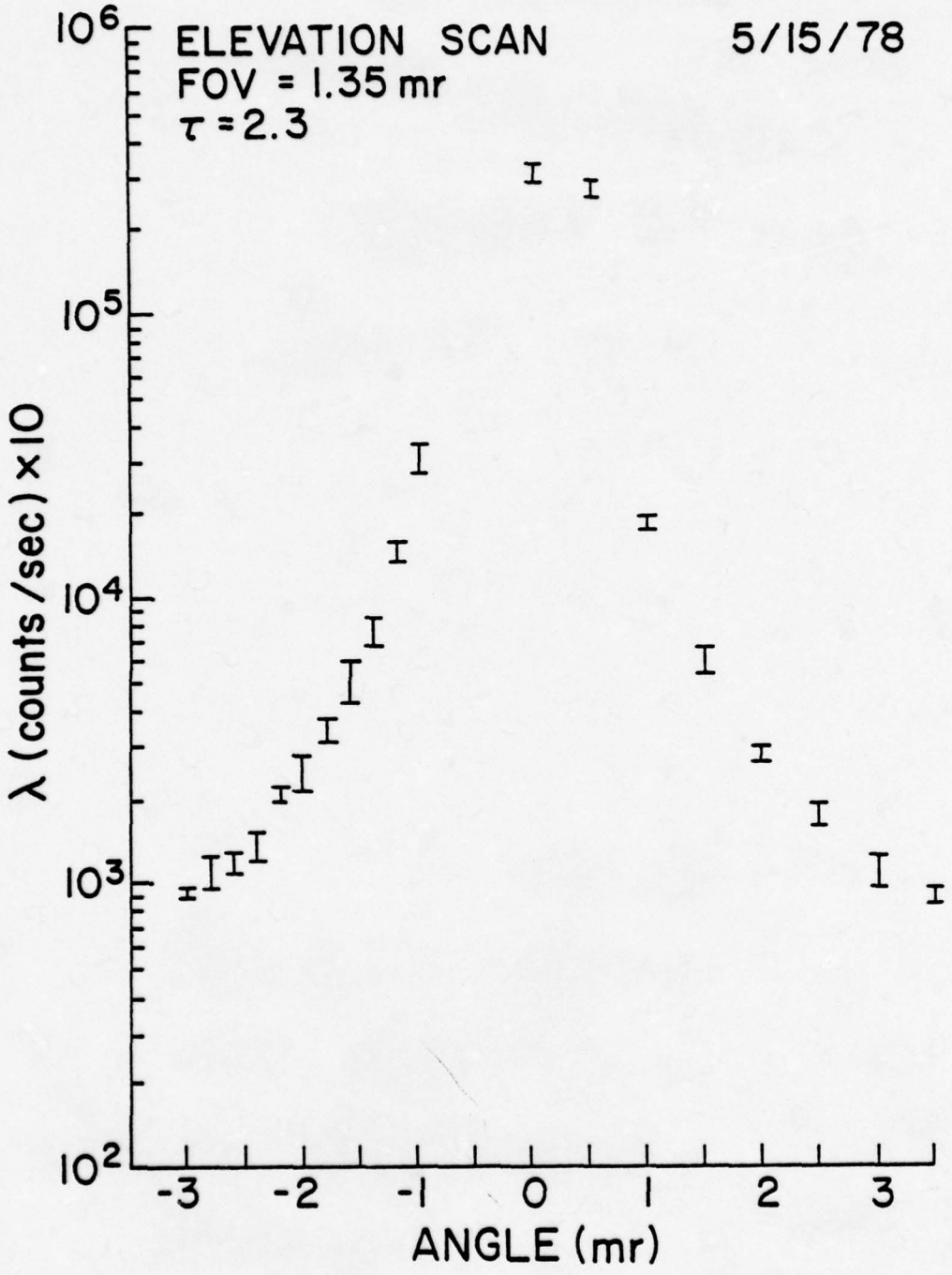
ELEVATION SCAN
5/15/78
FOV = 1.35 mr
τ = 2.3
λ (counts/sec) x10
10^6
10^5
10^4
10^3
10^2
-3
-2
-1
0
1
2
3
ANGLE (mr)

Fig. A-2

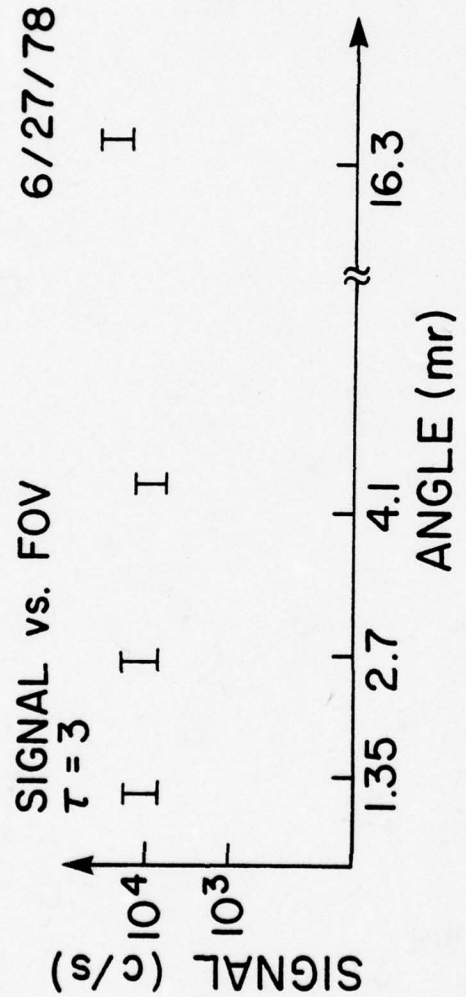

Fig. A-3

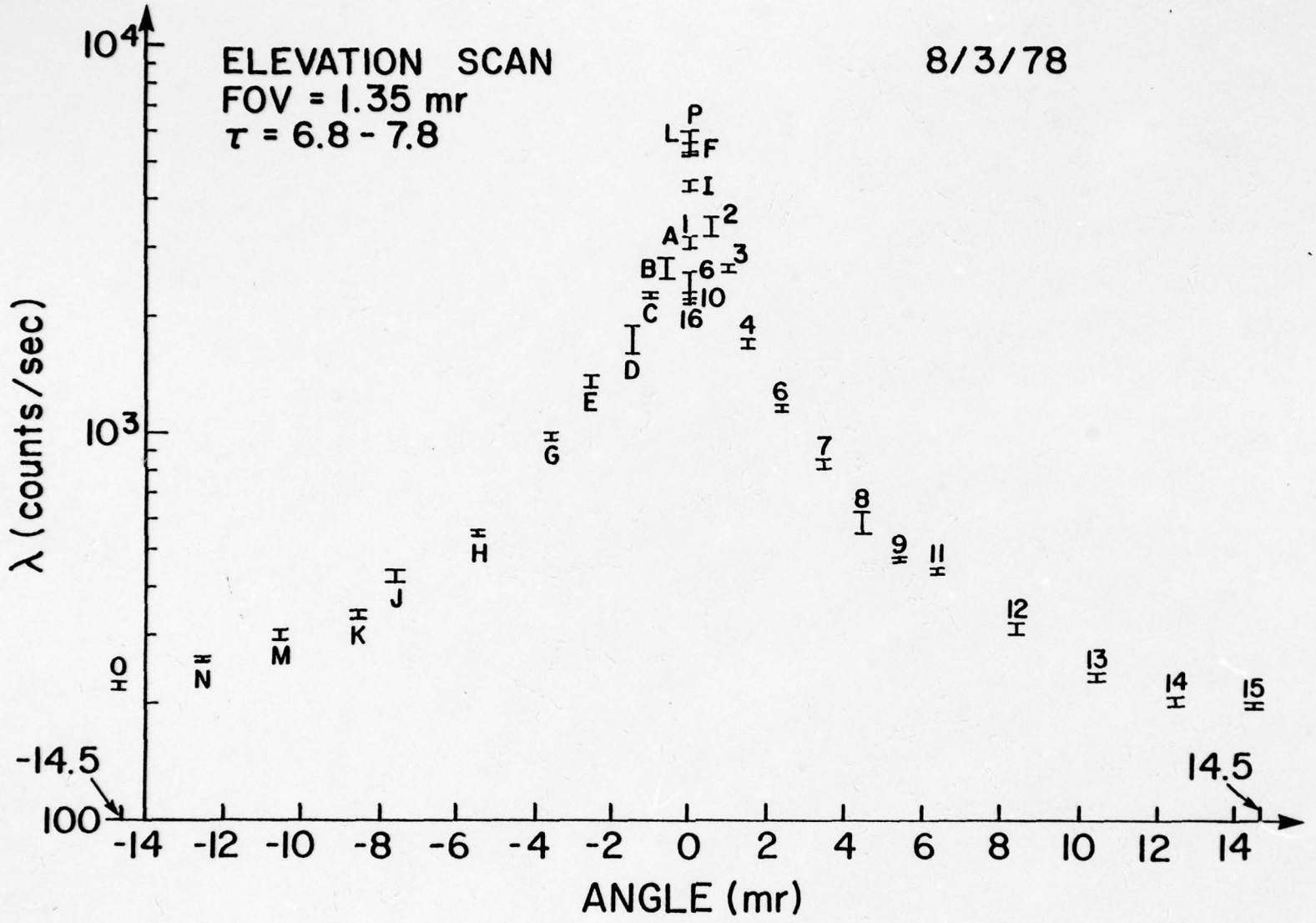
ELEVATION SCAN
FOV = 1.35 mr
τ = 6.8 - 7.8
8/3/78
λ (counts/sec)
10⁴
10³
100
-14.5
14.5
-14 -12 -10 -8 -6 -4 -2 0 2 4 6 8 10 12 14
ANGLE (mr)

Fig. A-4

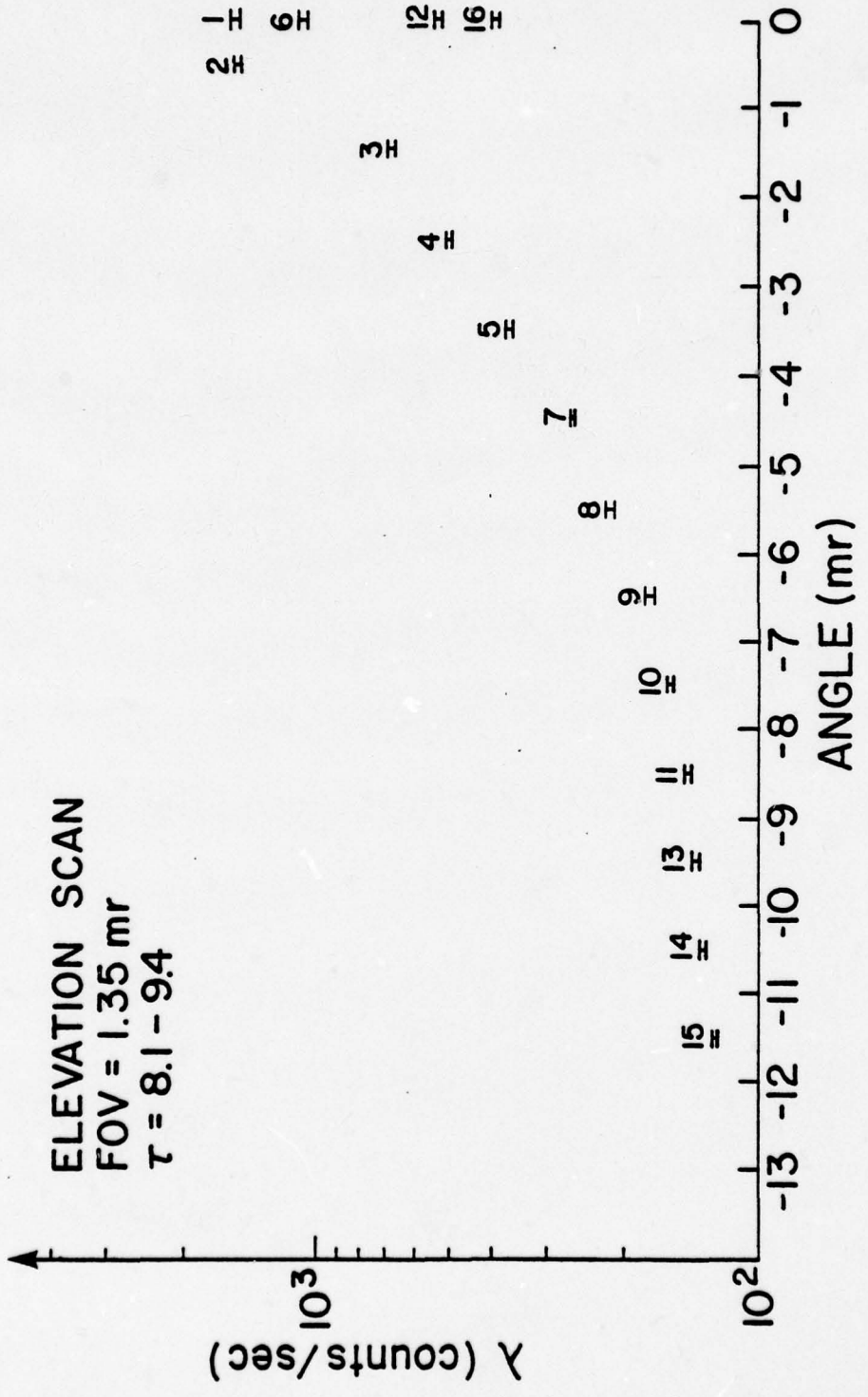
ELEVATION SCAN
FOV = 1.35 mr
τ = 8.1 - 9.4
λ (counts/sec)
10^3
10^2
0 -1 -2 -3 -4 -5 -6 -7 -8 -9 -10 -11 -12 -13
ANGLE (mr)
1
2
3
4
5
6
7
8
9
10
11
12
13
14
15
16

Fig. A-5

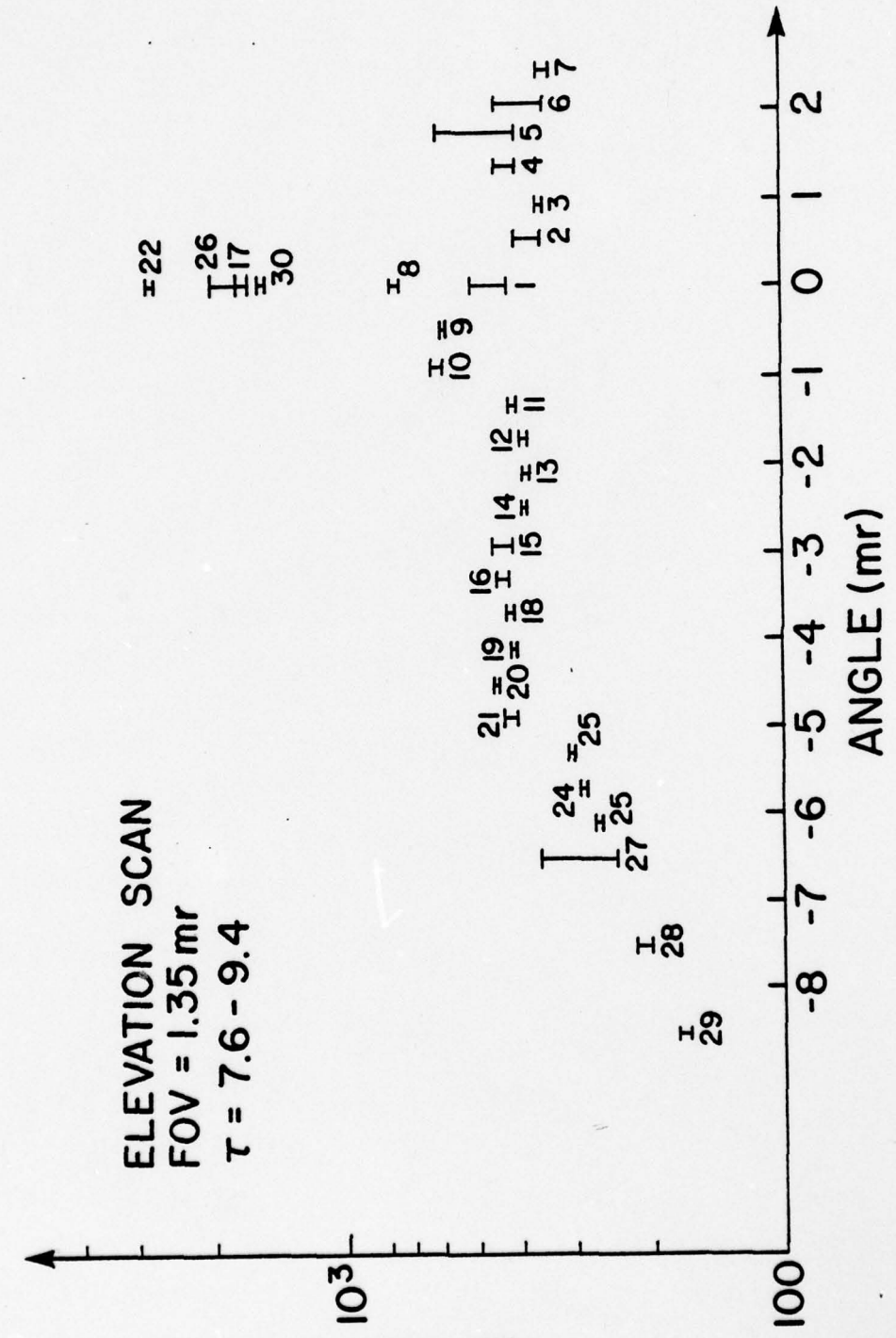
ELEVATION SCAN
FOV = 1.35 mr
τ = 7.6 - 9.4
λ (counts/sec)
10³
100
-8 -7 -6 -5 -4 -3 -2 -1 0 1 2
ANGLE (mr)

Fig. A-6

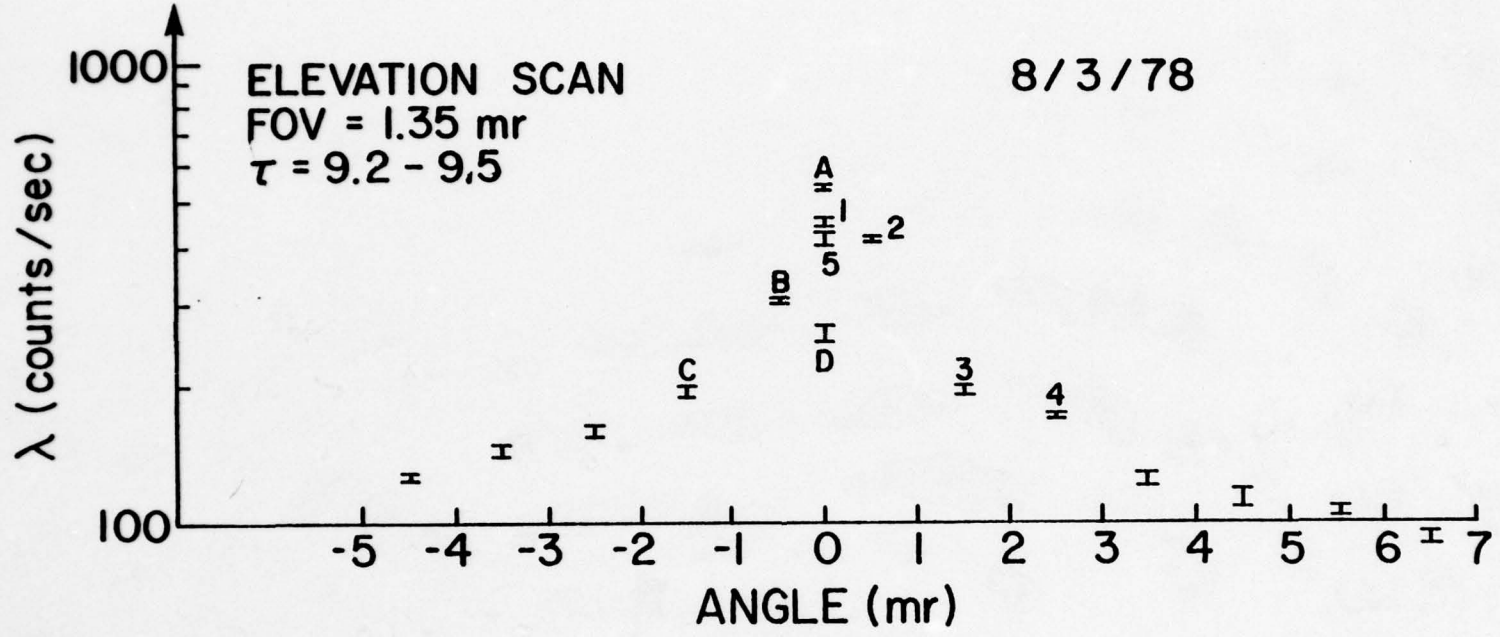
ELEVATION SCAN
8/3/78
FOV = 1.35 mr
τ = 9.2 - 9.5
λ (counts/sec)
1000
100
-5 -4 -3 -2 -1 0 1 2 3 4 5 6 7
ANGLE (mr)
A
1
2
5
B
D
C
3
4

Fig. A-7

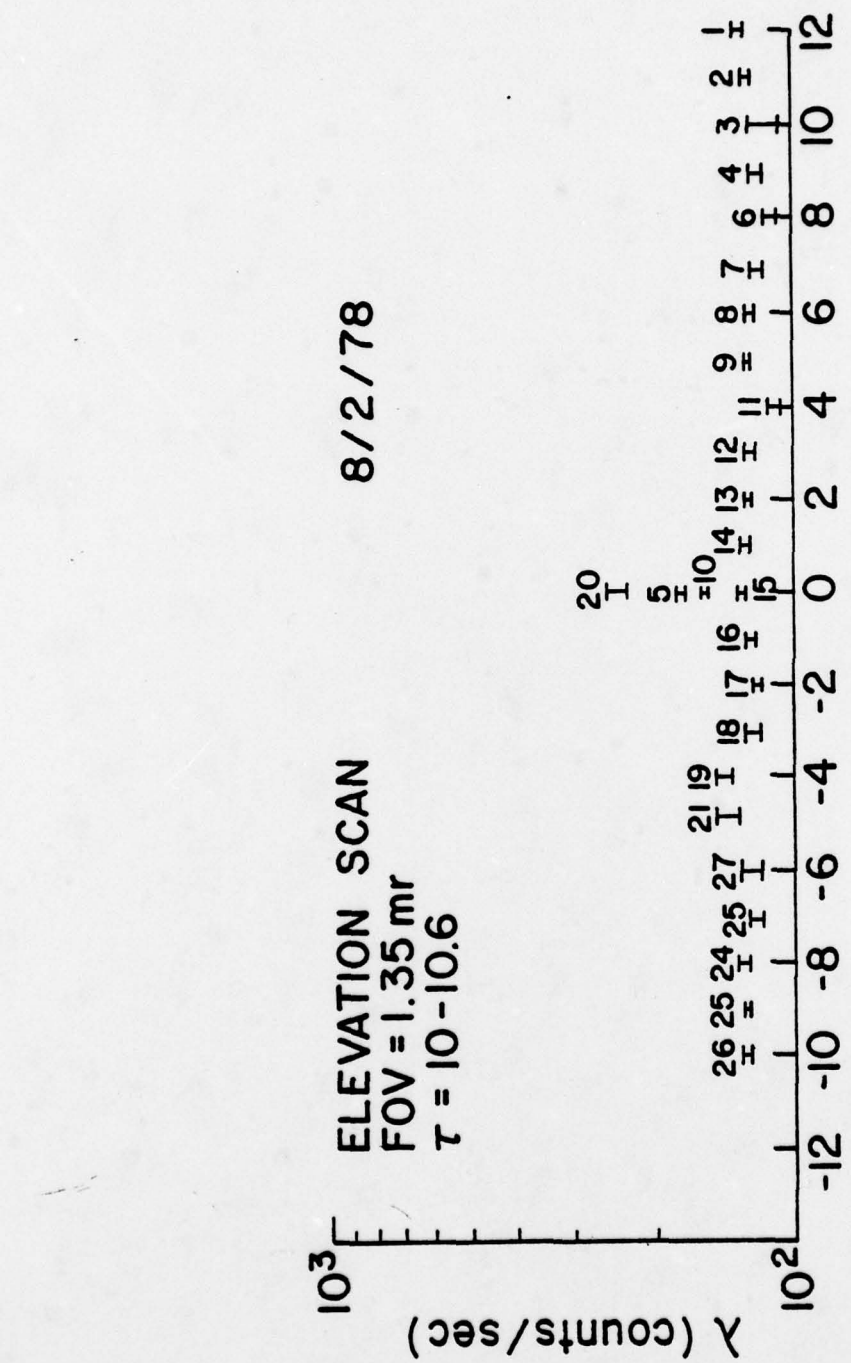
ELEVATION SCAN
FOV = 1.35 mr
τ = 10-10.6
8/2/78
λ (counts/sec)
10³
10²
ANGLE (mr)
-12
-10
-8
-6
-4
-2
0
2
4
6
8
10
12

Fig. A-8

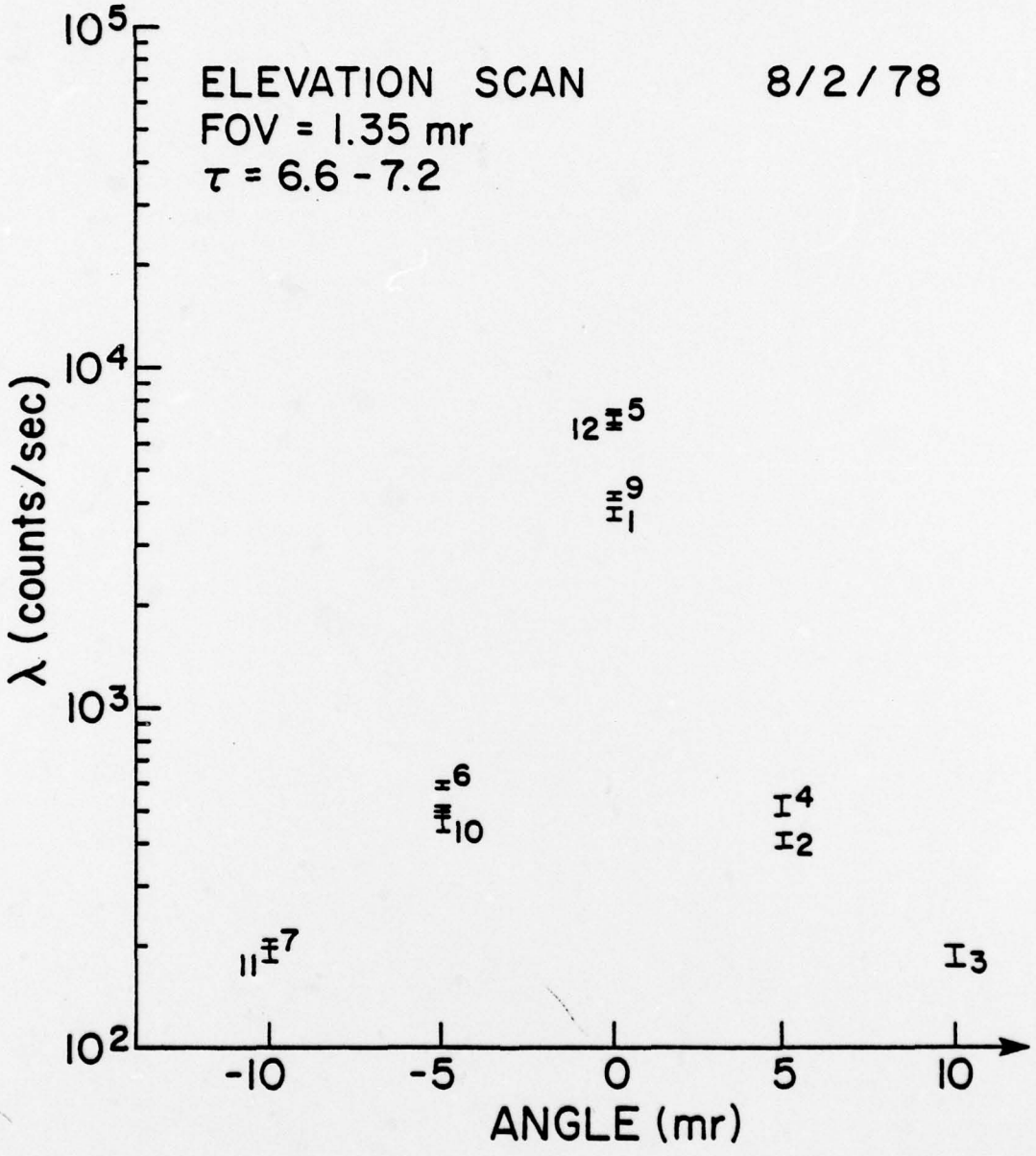
ELEVATION SCAN
8/2/78
FOV = 1.35 mr
τ = 6.6 - 7.2
λ (counts/sec)
10^5
10^4
10^3
10^2
12 II 5
II 9
1
II 6
10
I 4
I 2
11 II 7
I 3
-10
-5
0
5
10
ANGLE (mr)

Fig. A-9

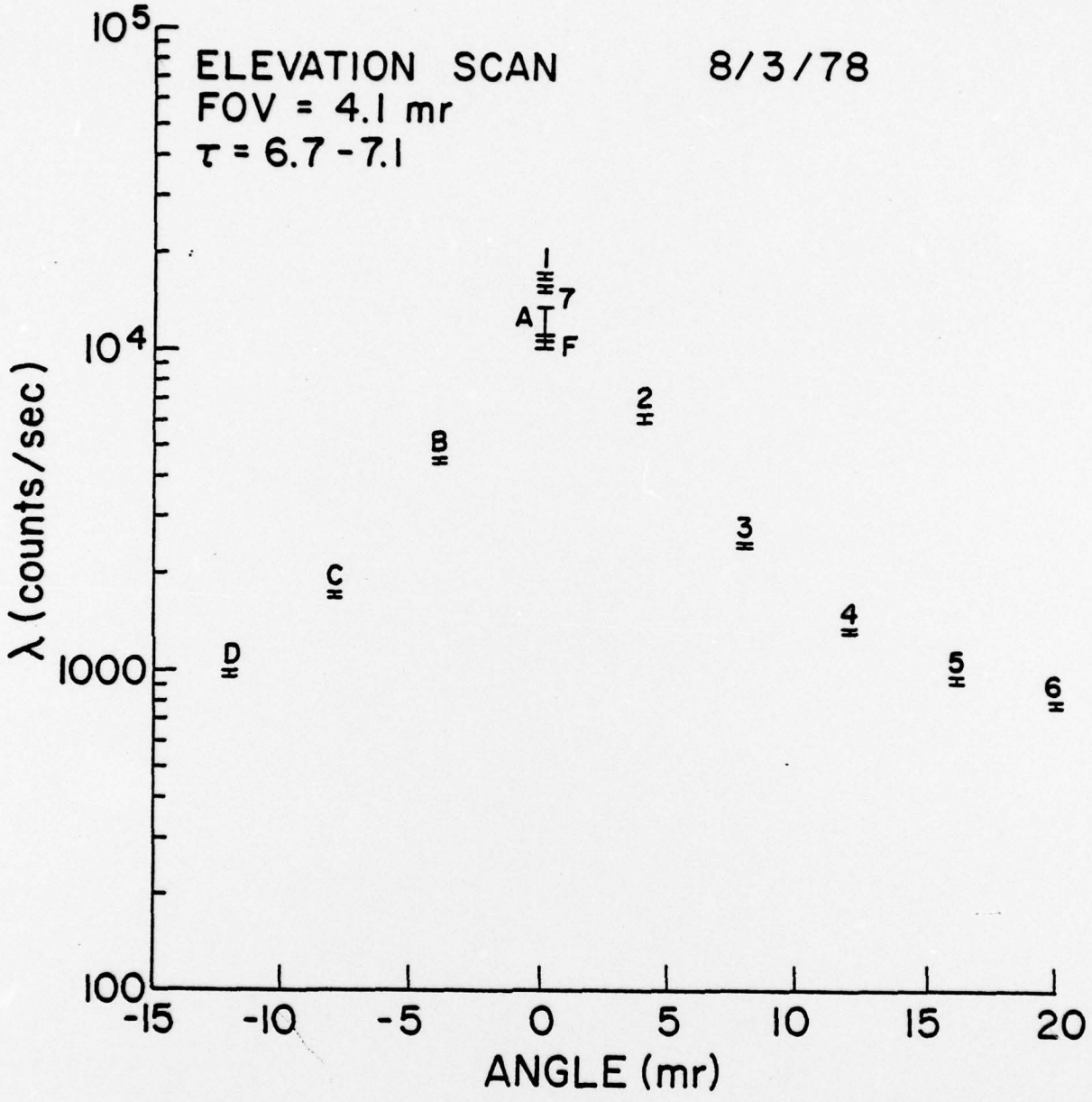
ELEVATION SCAN
8/3/78
FOV = 4.1 mr
τ = 6.7 - 7.1
λ (counts/sec)
10^5
10^4
1000
100
-15
-10
-5
0
5
10
15
20
ANGLE (mr)
A
B
C
D
F
1
2
3
4
5
6
7

Fig. A-10

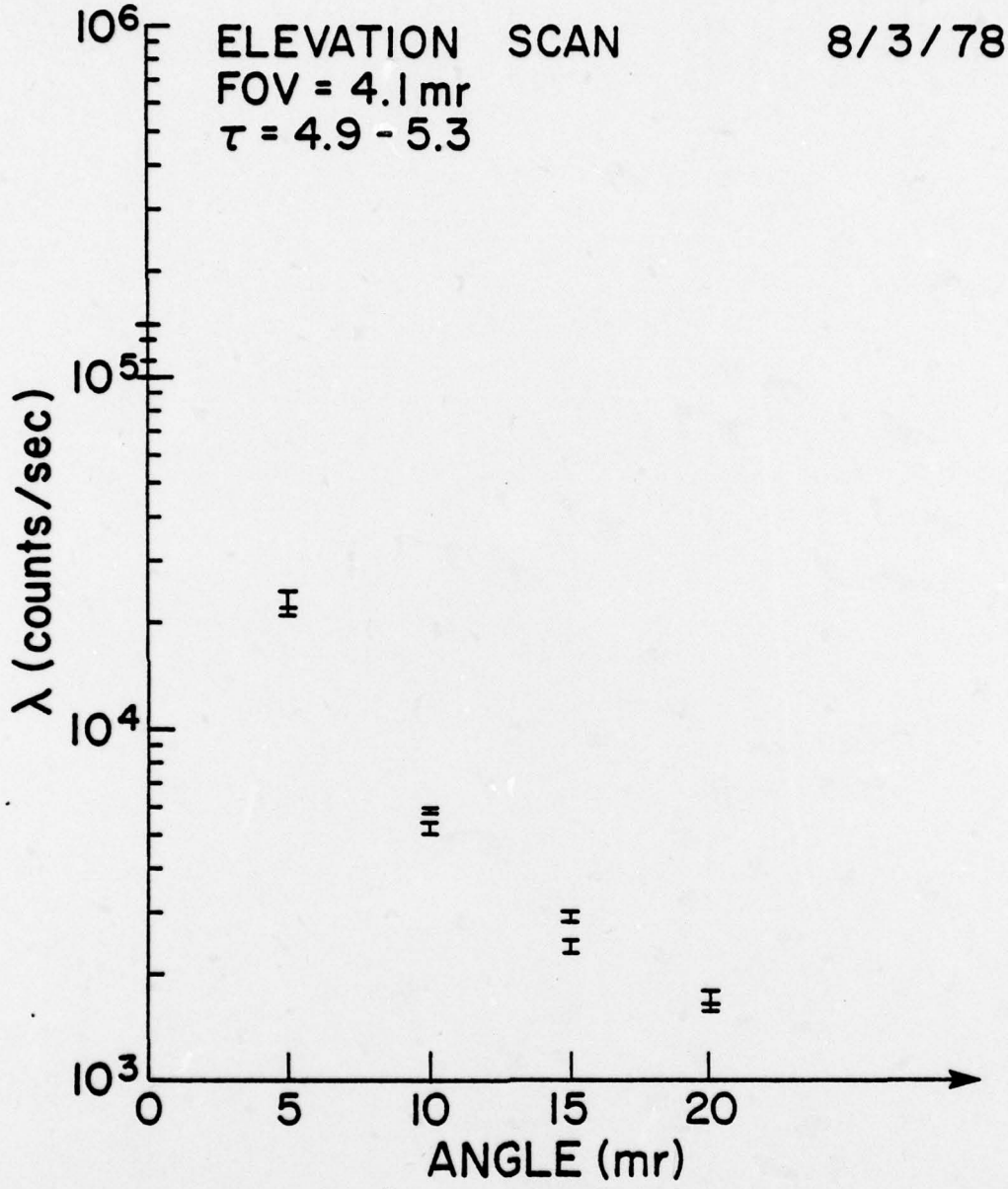
ELEVATION SCAN
8/3/78
FOV = 4.1 mr
τ = 4.9 - 5.3
λ (counts/sec)
10^6
10^5
10^4
10^3
0
5
10
15
20
ANGLE (mr)

Fig. A-11

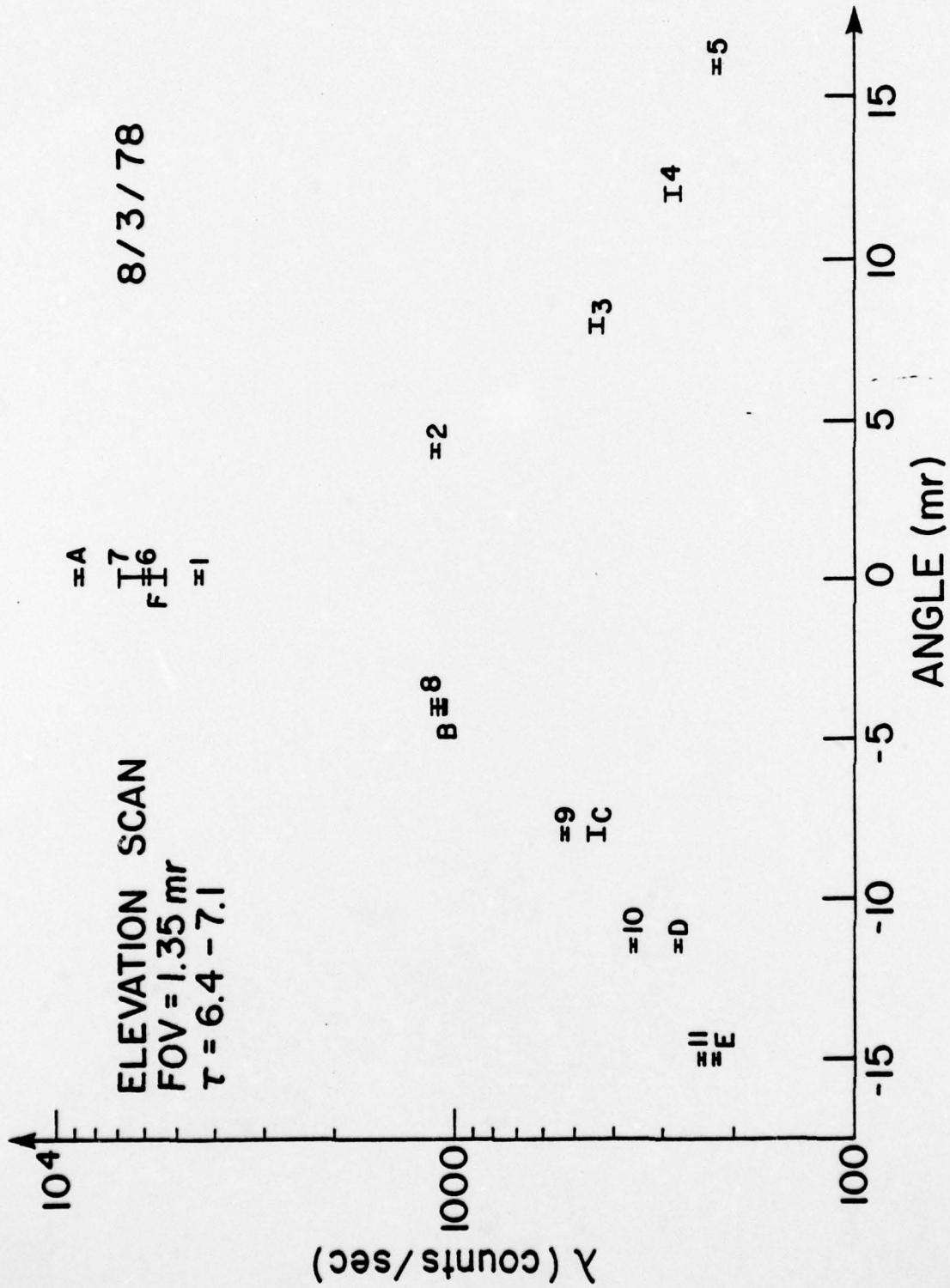
ELEVATION SCAN
FOV = 1.35 mr
τ = 6.4 - 7.1
8/3/78
λ (counts/sec)
ANGLE (mr)
10⁴
1000
100
-15
-10
-5
0
5
10
15
=A
=1
=2
=5
=9
=10
=D
=11
=E
B≡8
I3
I4
Ic

Fig. A-12

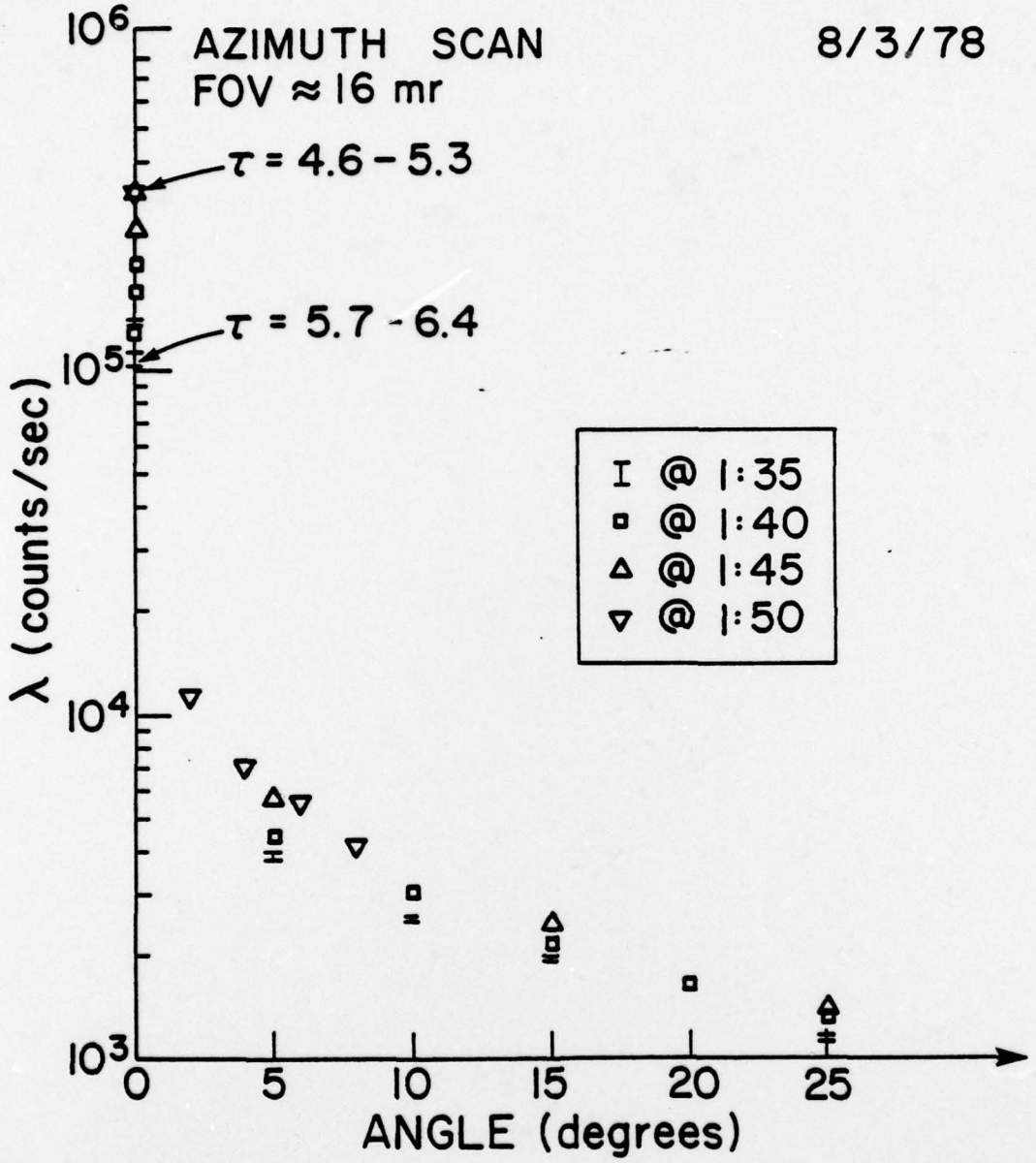
AZIMUTH SCAN
8/3/78
FOV ≈ 16 mr
τ = 4.6 - 5.3
τ = 5.7 - 6.4
I @ 1:35
@ 1:40
@ 1:45
@ 1:50
λ (counts/sec)
10^6
10^5
10^4
10^3
0
5
10
15
20
25
ANGLE (degrees)

Fig. A-13

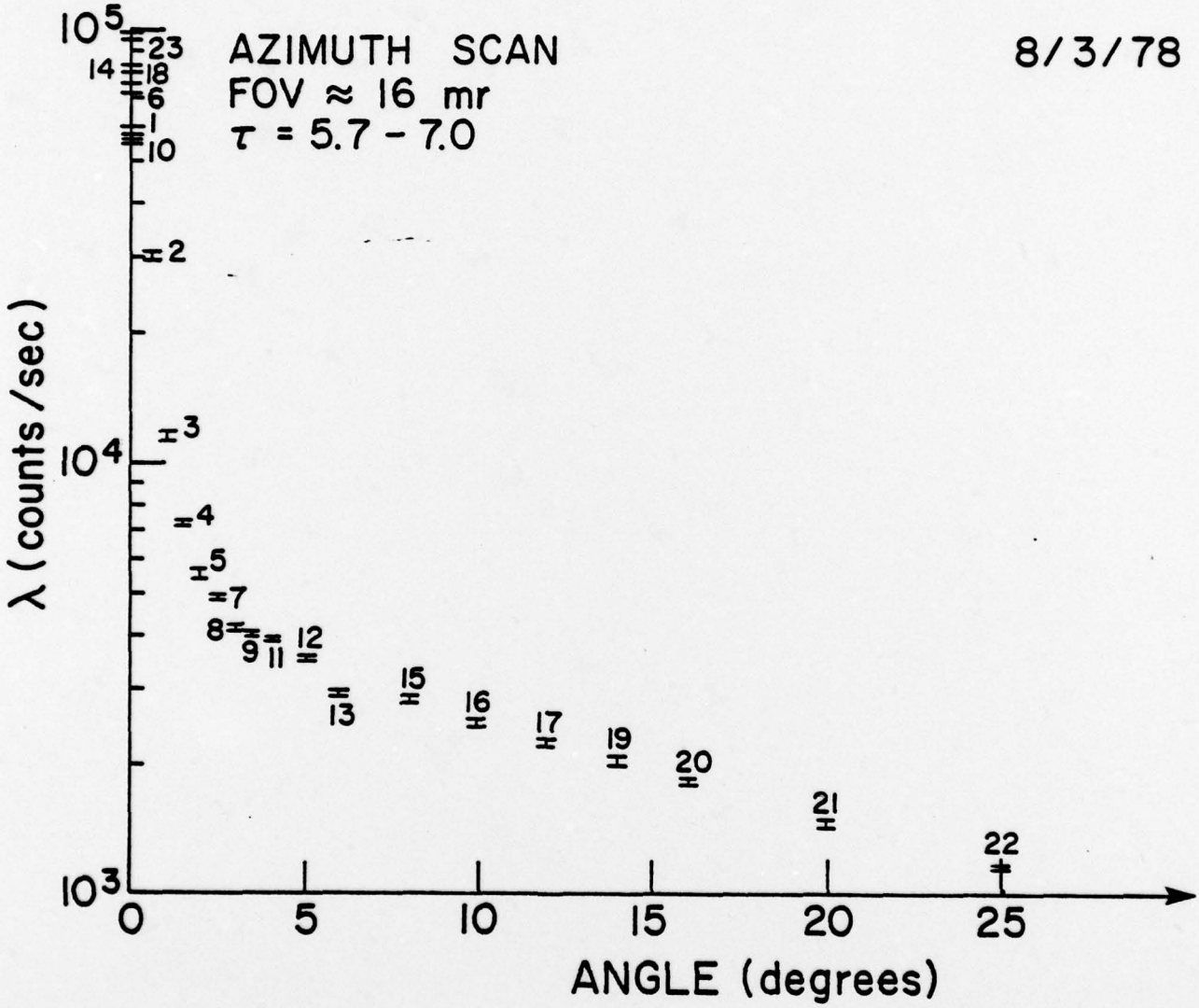
AZIMUTH SCAN
FOV ≈ 16 mr
τ = 5.7 - 7.0
8/3/78
λ (counts/sec)
10^5
10^4
10^3
0
5
10
15
20
25
ANGLE (degrees)
23
14
18
6
1
10
2
3
4
5
7
8
9
11
12
13
15
16
17
19
20
21
22

Fig. A-14

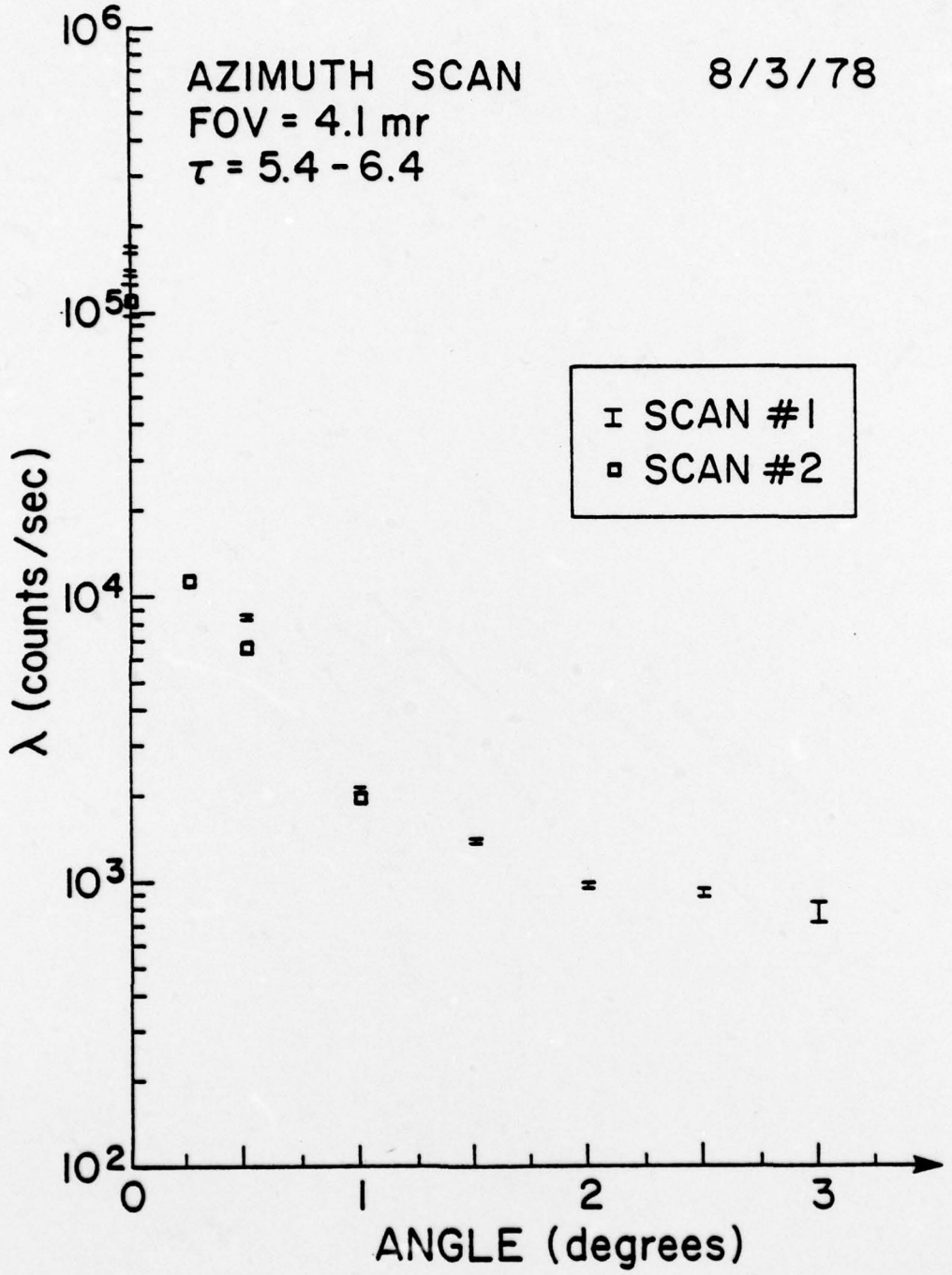
AZIMUTH SCAN
8/3/78
FOV = 4.1 mr
τ = 5.4 - 6.4
SCAN #1
SCAN #2
λ (counts/sec)
10^6
10^5
10^4
10^3
10^2
0
1
2
3
ANGLE (degrees)

Fig. A-15

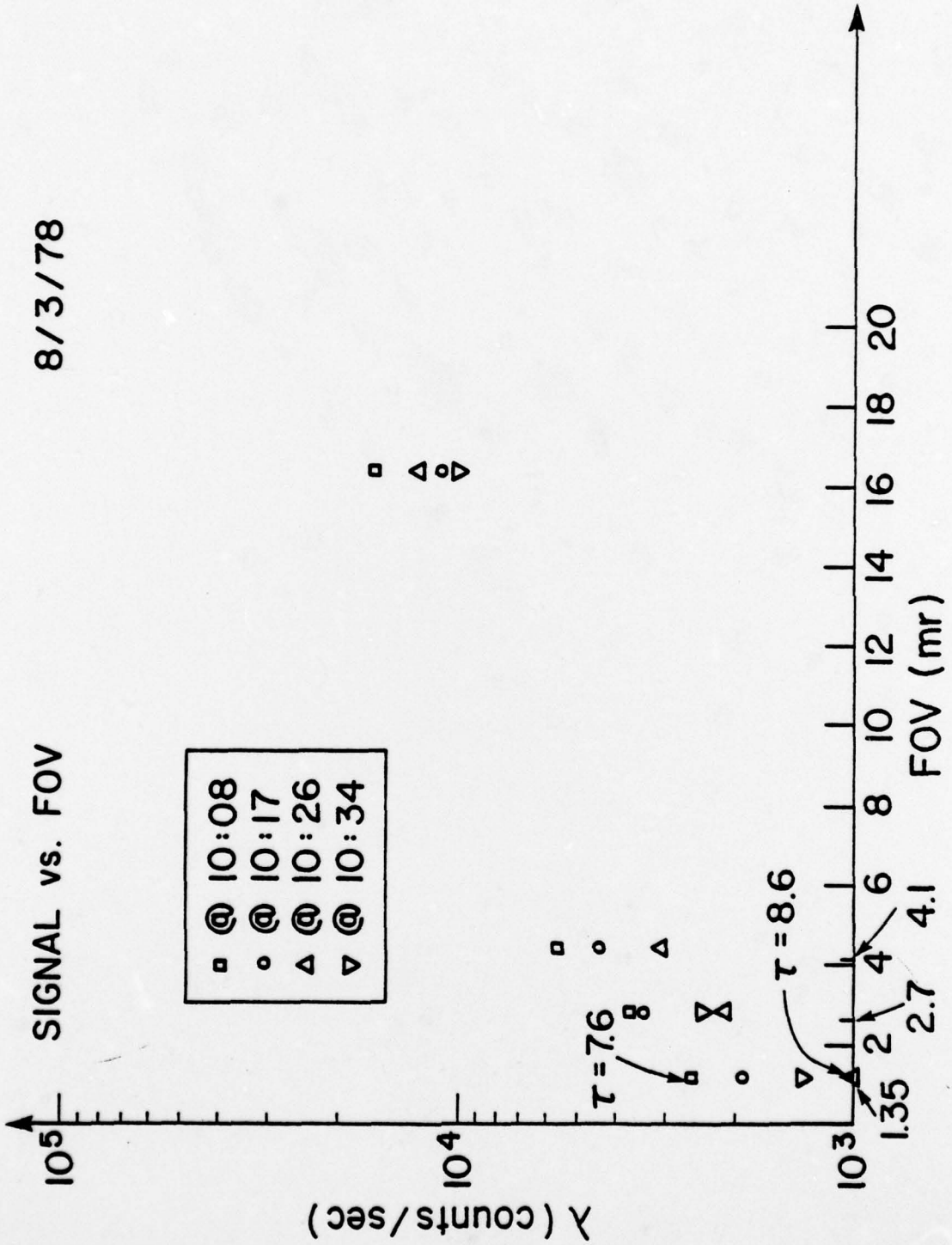
SIGNAL vs. FOV
8/3/78
@ 10:08
@ 10:17
@ 10:26
@ 10:34
λ (counts/sec)
10^5
10^4
10^3
FOV (mr)
2
4
6
8
10
12
14
16
18
20
1.35
2.7
4.1
τ=7.6
τ=8.6

Fig. A-16

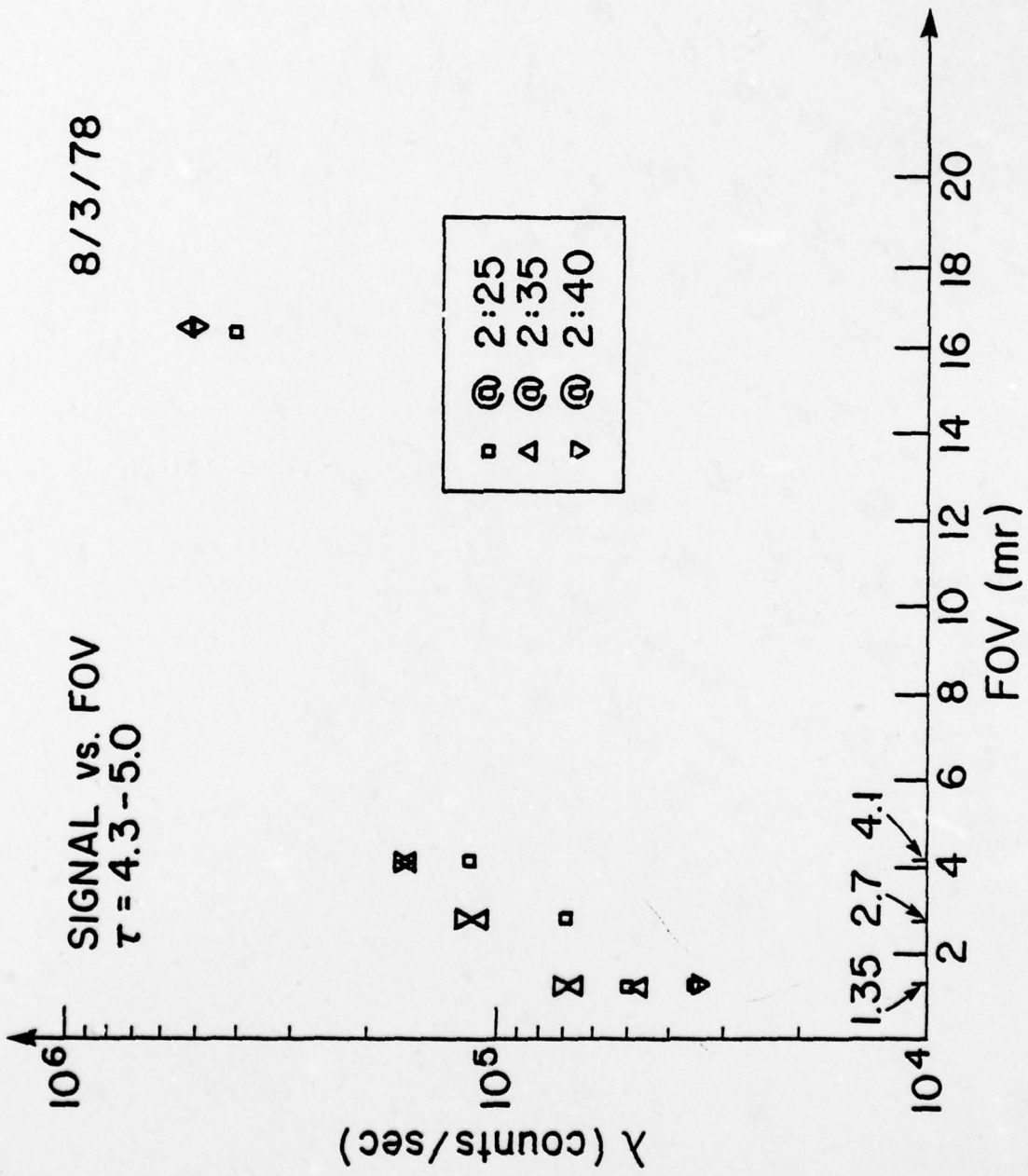
SIGNAL vs. FOV
τ = 4.3-5.0
8/3/78
▫ @ 2:25
△ @ 2:35
▷ @ 2:40
λ (counts/sec)
10^6
10^5
10^4
1.35
2.7
4.1
2
4
6
8
10
12
14
16
18
20
FOV (mr)

Fig. A-17

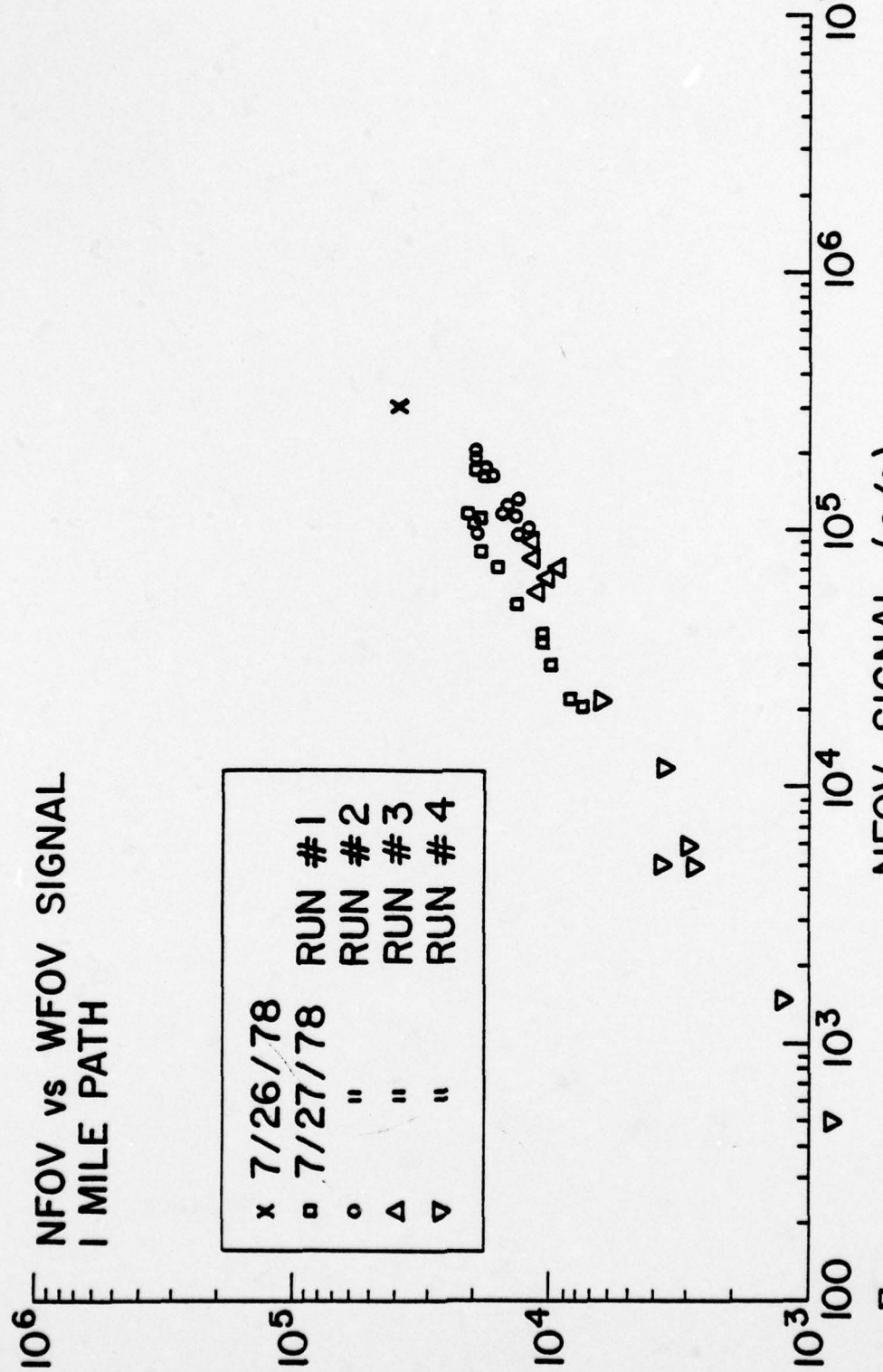
NFOV vs WFOV SIGNAL
1 MILE PATH
× 7/26/78
▫ 7/27/78 RUN #1
○ " RUN #2
△ " RUN #3
▽ " RUN #4
WFOV SIGNAL (c/s)
NFOV SIGNAL (c/s)
10^6
10^5
10^4
10^3
100
10^3
10^4
10^5
10^6
10^7

Fig. A-18

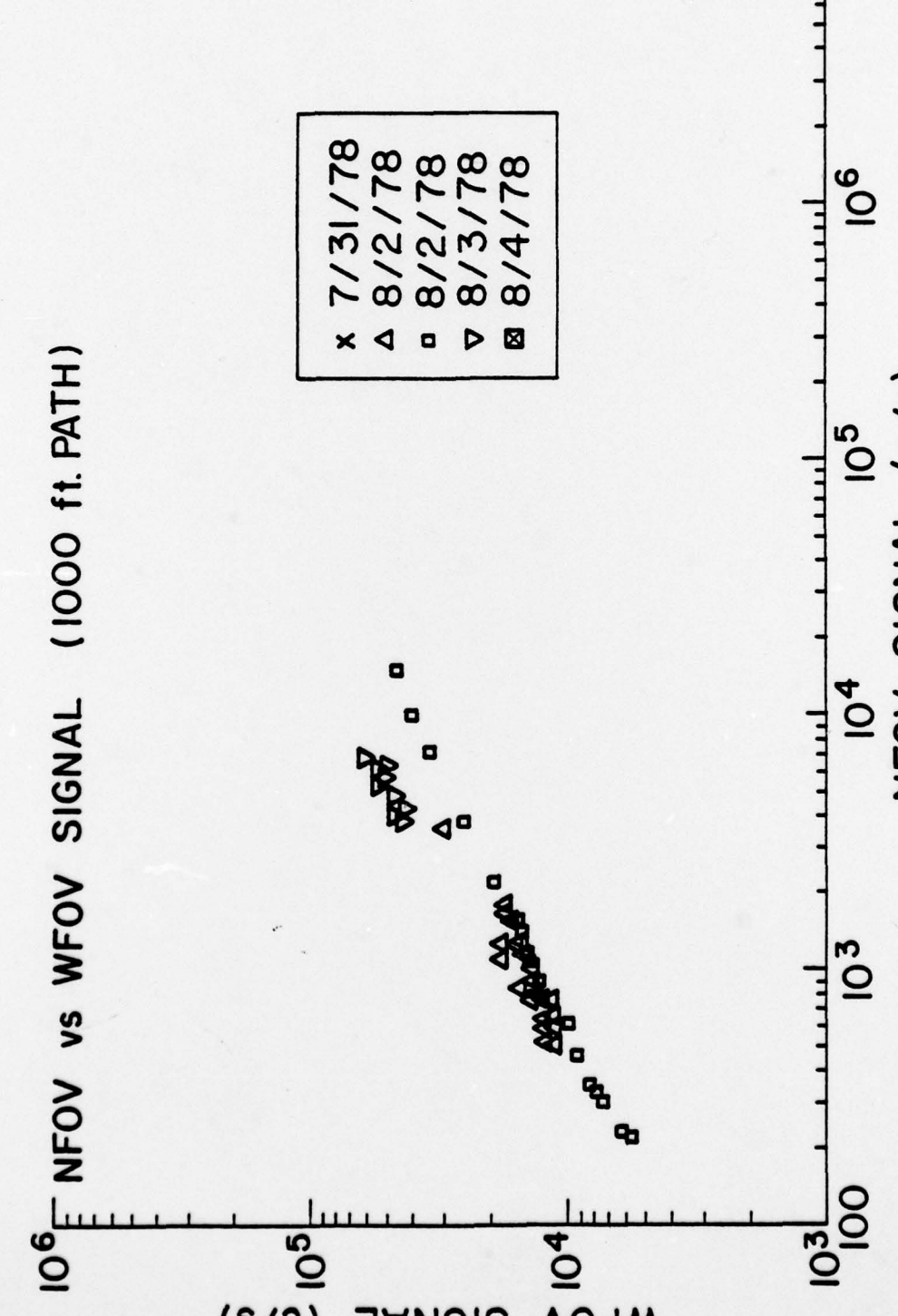
NFOV vs WFOV SIGNAL (1000 ft. PATH)
WFOV SIGNAL (c/s)
NFOV SIGNAL (c/s)
10^6
10^5
10^4
10^3
100
10^3
10^4
10^5
10^6
10^7
x 7/31/78
△ 8/2/78
▫ 8/2/78
▽ 8/3/78
⊠ 8/4/78

Fig. A-19

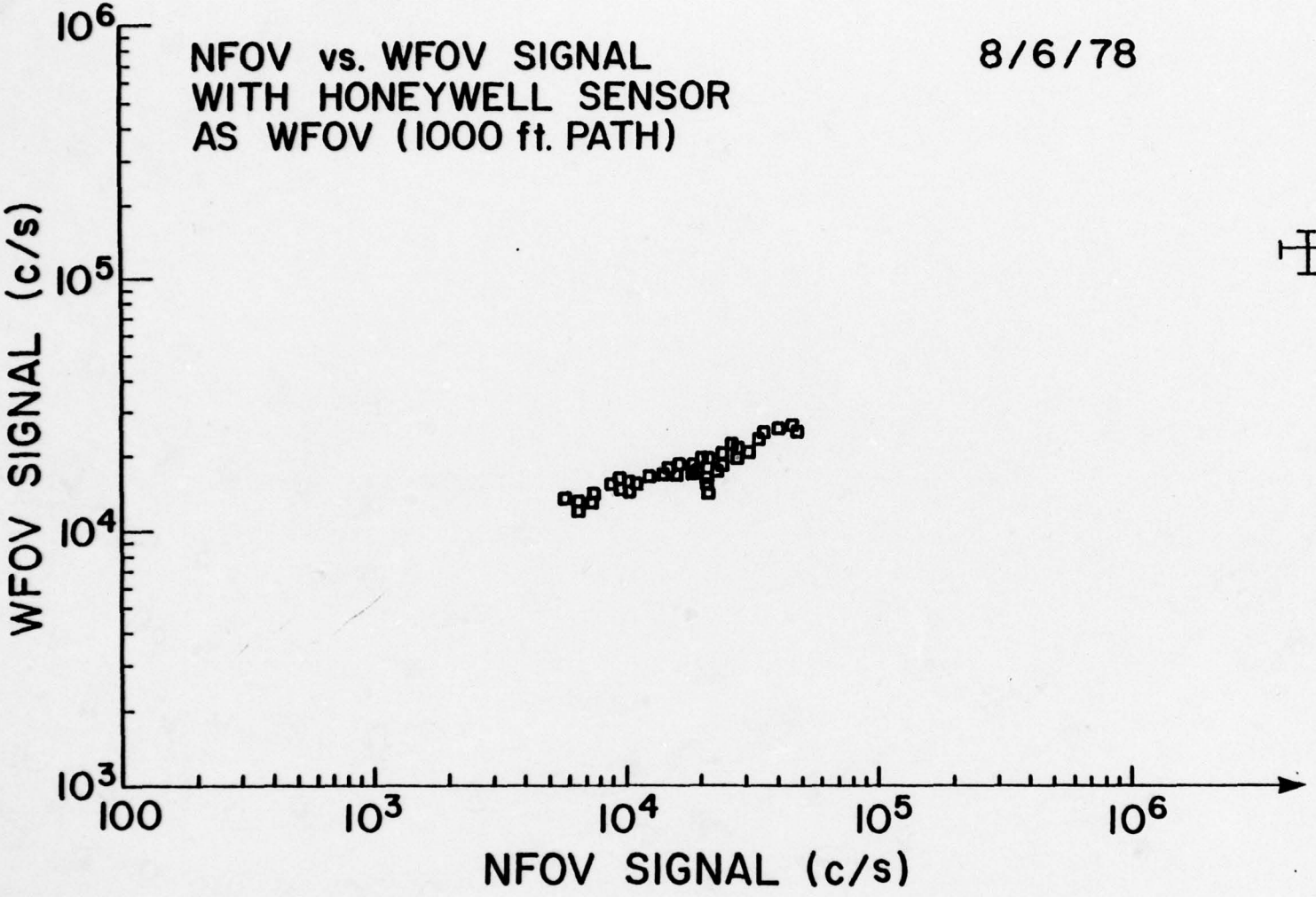
NFOV vs. WFOV SIGNAL
WITH HONEYWELL SENSOR
AS WFOV (1000 ft. PATH)
8/6/78
WFOV SIGNAL (c/s)
10^6
10^5
10^4
10^3
100
10^3
10^4
10^5
10^6
NFOV SIGNAL (c/s)

Fig. A-20